https://ntrs.nasa.gov/search.jsp?R=20180000709 2019-04-29T09:50:56+00:00Z

New Insights about Cloud Vertical Structure from CloudSat and CALIPSO observations

By

Lazaros Oreopoulos[1], Nayeong Cho[2,1], and Dongmin Lee[3,1]

1. NASA-GSFC, Earth Science Division, Greenbelt MD 20771 USA

2. USRA, Columbia, MD 21044 USA

3. Morgan State University, Baltimore MD 21251 USA

Revised for the Journal of Geophysical Research-Atmospheres

June 2017

Key points:

(1) Complex cloud vertical structure (CVS) can be reduced to a few major classes

(2) These CVS classes vary substantially in space and time and have very distinct radiative effects

(3) Previous interpretations of cloud regimes from passive observations are largely consistent with the blend of CVS classes they consist of

Corresponding Author:
Lazaros Oreopoulos
Earth Science Division, Code 613
NASA-GSFC
Greenbelt MD 20771
USA
e-mail: Lazaros.Oreopoulos@nasa.gov
phone: +1 301-614-6128

Abstract

Active cloud observations from A-Train's CloudSat and CALIPSO satellites offer new opportunities to examine the vertical structure of hydrometeor layers. We use the 2B-CLDCLASS-LIDAR merged CloudSat-CALIPSO product to examine global aspects of hydrometeor vertical stratification. We group the data into major Cloud Vertical Structure (CVS) classes based on our interpretation of how clouds in three standard atmospheric layers overlap, and provide their global frequency of occurrence. The two most frequent CVS classes are single-layer (per our definition) low and high clouds which represent ~53% of cloudy skies, followed by high clouds overlying low clouds, and vertically extensive clouds that occupy near-contiguously a large portion of the troposphere. The prevalence of these configurations changes seasonally and geographically, between daytime and nighttime, and between continents and oceans. The radiative effects of the CVS classes reveal the major radiative warmers and coolers from the perspective of the planet as a whole, the surface, and the atmosphere. Single-layer low clouds dominate planetary and atmospheric cooling, and thermal infrared surface warming. We also investigate the consistency between passive and active views of clouds by providing the CVS breakdowns of MODIS cloud regimes for spatiotemporally coincident MODIS-Aqua (also on the A-Train) and CloudSat-CALIPSO daytime observations. When the analysis is expanded for a more in-depth look at the most heterogeneous of the MODIS cloud regimes, it ultimately confirms previous interpretations of their makeup that did not have the benefit of collocated active observations.

1. Introduction

It becomes immediately obvious even to the most casual observer that cloud morphology is rich, variable, and complex. Satellite observations have been essential in our effort to describe and devise measures to quantify a variety of cloud characteristics. Measurements by CloudSat's Cloud Precipitation Radar [CPR, *Stephens et al. 2002*] and CALIPSO's Cloud-Aerosol Lidar with Orthogonal Polarization [CALIOP, *Winker et al. 2010*], both members of the A-Train satellite constellation *[L'Ecuyer and Jiang 2010]*, have been instrumental in this effort as they have brought new insights about hydrometeor (cloud and precipitation particles) salient features that remained elusive when relying on only the passive imagers and microwave radiometers at our disposal. In short, these two CloudSat-CALIPSO (CC) active sensors have yielded breakthroughs in our knowledge of hydrometeor vertical variability, structure, and overlap, greatly extending what can be achieved solely with passive sensors [*Chang and Li 2005a,b; Joiner et al. 2010; Wind et al. 2010*]. The new information has allowed us to examine, among others: the details of cloud overlap in a manner suitable for parameterization in Large Scale Models [*Barker 2008*; *Shonk et al. 2010*; *Oreopoulos et al. 2012*], the contribution of different cloud systems to the radiative heating/cooling profiles of the atmosphere (*Haynes et al. 2013*; *Oreopoulos et al. 2016*), and the (in)consistency between passive and active views of clouds (*Mace and Wrenn 2013*; *Leinonen et al. 2016*).

Following along the lines of previous work (such as *Mace et al.* 2009; *Li et al.* 2015), this paper also focuses on Cloud Vertical Structure (CVS) as seen jointly by CPR and CALIOP. As explained in *Mace et al.* [*2009*], the 94 GHz W-Band CPR can probe rather deeply into hydrometeor layers before being attenuated in the presence of rain, and sometimes has

difficulty distinguishing between cloud and precipitation particles. CALIOP, on the other hand, is very sensitive to even thin cloud layers, but cannot probe the details of the atmosphere below clouds of even modest optical thickness (~3 from cloud top). Nevertheless, these two instruments provide jointly the most complete hitherto picture of cloud vertical arrangements. We take advantage of this ability, and aspire to provide a global climatology of CVS, a basic understanding of its main variability features, and why it matters radiatively. We also seek to understand how previous classifications of cloud systems based on passive observations relate to cloud groupings from a CVS perspective. Extracting and analyzing CVS from observations is important for a variety of reasons: (a) It allows us to determine and understand the influence of hydrometeors on the vertical distribution of radiative and latent energy across the globe and hence the atmospheric energy balance; (b) it provides clues about the flux of precipitation throughout the atmosphere; (c) it helps assess the limitations of cloud observations that do not resolve CVS; (d) it provides information that can prove valuable when assessing the realism of cloud simulations in numerical models such as cloud resolving models and Atmospheric General Circulation Models (AGCMs).

Because CVS can potentially be complex with many permutations of how distinct cloud layers overlap possible, simplifications are in order. Making the problem manageable is therefore a major aspect of the paper. While our CVS classes are exactly the same as those by *Tselioudis et al.* [*2013*], the data product they are obtained from and the derivation method differs from theirs. Similar to that paper, we examine what kind of CVS classes are contained in so-called cloud regimes from passive observations, an exercise that is very illuminating about how different observing systems see the same clouds. Another major aspect of our paper is

examining the effect of the different CVS classes on radiative fluxes. Because radiative fluxes are reconstructed from cloud information, investigation of the radiative effects of CVS classes does not have to be limited only to the Top of the Atmosphere (TOA). Rather, we can also determine what the radiative effects of the CVS classes are at the surface and within the atmosphere.

Our paper consists of two major parts: (1) global CVS climatology and associated global radiative effects; (2) investigation of the vertical structure (via CVS classes) of the Moderate Resolution Imaging Spectroradiometer (MODIS) cloud regimes of *Oreopoulos et al.* [2016]. These analyses are preceded by a description of how the CVS classes are derived. The assumptions and other details of the derivation are provided separately in an Appendix.

2. Datasets and Analysis Methodology

2.1 CVS class determination

Cloud Vertical Structure (CVS) can be quite intricate with many configurations possible, so distilling its essence into few manageable classes requires a considerable amount of judicious simplifications. We follow on the footsteps of *Tselioudis et al.* [*2013*], and use as a backbone the traditional International Satellite Cloud Climatology Project (ISCCP, *Rossow and Garder 1993*) classification which broadly assigns clouds into one of high (*H*), middle (*M*), and low (*L*) cloud categories based on cloud top location, with 680 hPa and 440 hPa serving as the atmospheric pressure boundaries delineating the three *standard layers* and associated cloud categories. In our case, this simple cloud classification can be modified to overcome ISCCP's limitations since

CloudSat and CALIPSO (especially when combined) provide in principle also cloud bottom information, and can distinguish between distinct cloud layers in the vertical.

We use four years (2007-2010) of the merged CloudSat/CALIPSO product 2B-CLDCLASS-LIDAR R04 [*Sassen and Wang 2012;* see also http://tinyurl.com/2b-cldclass-lidar] which contains atmospheric profiles with horizontal and vertical resolutions of 1.4x1.8 $(km)^2$ and 240 m, respectively, and extends from 82°S to 82°N. The information used from 2B-CLDCLASS-LIDAR is the heights of hydrometeor layer top and base in each profile; we consider those equivalent to the vertical locations of the boundaries of individual cloud elements. The aforementioned framework of three standard layers is then used to define the major CVS classes. To make the problem manageable, multiple cloud layers (i.e., separated by clear skies) are not considered as such when co-existing within a standard layer (they are reduced to single-layer); when two or more cloud elements belonging to one of the *H*, *M*, *L* cloud categories co-exist, they can be either contiguous or non-contiguous (separated by clear layers). With the above assumptions, the possible combinations that yield the same tractable set of CVS classes as *Tselioudis et al.* [*2013*] are (see Fig. 1): single-layer high clouds (H); single-layer middle clouds (M); single-layer low clouds (L); contiguous (or near-contiguous) clouds spanning the 440-680 hPa and <440 hPa standard layers (H×M); contiguous (or near-contiguous) clouds spanning the 440-680 hPa and >680 hPa standard layers (M×L); contiguous (or near-contiguous) clouds spanning all three standard layers (H×M×L); non-contiguous clouds co-occurring in the 440-680 hPa and <440 hPa standard layers (HM); non-contiguous clouds co-occurring in the <440 hPa and >680 hPa standard layers (HL); non-contiguous clouds co-occurring in the 440-680 hPa and >680 hPa standard layers (ML); and finally non-contiguous clouds simultaneously occurring in all three

standard layers (HML). These combinations form the 10 CVS “classes” (11 if clear skies are also counted) depicted in Fig. 1. The Appendix describes in more detail how the far more numerous possible permutations of cloud vertical co-occurrence in 2B-CLDCLASS-LIDAR are consolidated into these few classes. Without going into the details that the Appendix exhaustively documents, we should point cloud profiles assigned CVS classes that appear single-layer (H, M, L) or contiguous (H×M, M×L, and H×M×L) in Fig. 1 may in reality be multi-layer in 2B-CLDCLASS-LIDAR according to conventional definitions. This is clearly shown in several example configurations of Figs A2-A4 that are reduced to single-layer (confined to only one standard layer) or contiguous CVS classes because the clear-sky separation of the distinct cloudy layers is not wide enough, i.e., clouds are “near-contiguous” (criteria are described in the Appendix). Our simplifications and the exact meaning of our CVS classes should therefore be taken into consideration when comparing with other studies of CVS.

In order to derive the simplified CVS classification, we need information for both the cloud top and cloud base pressures (CTP and CBP, respectively). The 2B-CLDCLASS-LIDAR (as well as all other CloudSat or merged products) provide altitude information in terms of physical height. To convert height to atmospheric pressure we use the ancillary 2B-ECMWF-AUX product. After the conversion from height to pressure has been accomplished, we can proceed to assignment of the CVS class for each observed profile using the scheme described in the Appendix.

We must note that we tested several variations of the procedure described in the Appendix, such as different pressure thickness thresholds for distinguishing between thick and thin clouds spanning two or three standard layers, and using CTP instead of the pressure at the geometrical center of the cloud entity to forcibly confine thin clouds spanning two standard

layers to a single standard layer. Remarkably, we found that global results were not too sensitive to specific choices. When the assignment of cloud configurations to the CVS classes per the scheme described in the Appendix was completed, we ended up with only 0.5% of cloudy columns (profiles) unassigned because of extreme complexity.

2.2 Radiative fluxes

The radiative impact of the different CVS categories is examined with the aid of the coincident 2B-FLXHR-LIDAR R04 data [*L'Ecuyer et al. 2008; Henderson et al. 2013; Matus and L'Ecuyer 2017*]. The impact is measured in terms of the SW and LW Cloud Radiative Effects (CREs), namely the difference between cloudy-sky and clear-sky net (downward minus upward) fluxes at the Top of the Atmosphere (TOA) and Bottom of the Atmosphere (BOA). The SW CREs are highly-dependent on the incoming solar flux at the time of the approximate 1:30 pm local solar time overpass, and are scaled to diurnal fluxes by normalizing with the ratio of the diurnally averaged incoming solar flux at TOA $\overline{F_{SW}^{TOA}}$ to the instantaneous incoming flux at TOA F_{SW}^{TOA} for that location and day of the year [as in *Haynes et al. 2013*]:

$$\overline{CRE}_{SW} = CRE_{SW}\left(\frac{\overline{F_{SW}^{TOA}}}{F_{SW}^{TOA}}\right) \quad (1)$$

This quantity is negative at both TOA and BOA when CRE is defined in terms of net fluxes, indicating that clouds cool both the Earth-Atmosphere system and the surface in the SW. The LW CREs, which are positive for both TOA and BOA indicating that the cloud thermal infrared (greenhouse) effect warms both the Earth-Atmosphere system and the surface, are not adjusted for diurnal variations (it is not clear or straightforward how to do this, and it matters

much less than for the SW). The sum of SW and LW CRE gives the "total" CRE (sometimes referred in the literature as "net" CRE). The difference between total CRE at the TOA and BOA gives the atmospheric (ATM) total CRE, an indicator of radiative warming or cooling.

2.3 MODIS CRs

We also use the MODIS Cloud Regimes (CRs) of *Oreopoulos et al.* [2016], hereafter O16. These come from International Satellite Cloud Climatology Project (ISCCP)-like daily (daytime) joint histograms of CTP and Cloud Optical Thickness (COT). To derive the CRs, the joint histograms from both Terra and Aqua were treated as a single ensemble that was subjected to *k-means* clustering analysis [*Rossow et al. 2005*] from which 12 global MODIS CRs emerged. Details can be found in O16. The regime centroids (mean of alike histograms) are displayed in Fig. 2 (same as Fig. 1 in O16). In addition, a brief overview of the salient characteristics of each MODIS CR and mean properties is provided in Table 1 (similar to Table 1 in *Oreopoulos et al.* [2017]).

In addition to the nominal CRs in O16 we explore internal variability of CR CVS occurrence, by further breaking these CRs into "subregimes" [*Mason et al.* 2014; *Leinonen et al.* 2016]. This is accomplished by using the Euclidean distances of CR member histograms from their CR centroid (mean histogram). Specifically, we create three subregimes for each CR by averaging all member histograms that have distances belonging to either the first (1q), the second (2q) or the third (3q) quartile of the distance distribution. There are other ways to create subregimes such as re-clustering all member histograms of a CR, but we found that the simple method based on the quartile grouping of distances produces meaningful distinct subregimes.

Moreover, we are mainly interested in the internal variability of a CR's CVS, and examining the problem from the perspective of subregimes is just one of several possible options.

3. Global Cloud Vertical Structure

3.1 Global climatology

Figure 3 shows the global area-weighted relative frequency of occurrence (RFO), in percentage, of the 11 (including clear skies) CVS classes. Since the RFO of a CVS class comes from the ratio of the number of cloudy columns belonging to the class to the total number of columns (appropriately weighted by area), on a global scale it has the same meaning as cloud fraction (CF). The x-axis shows cumulative RFO as CVS classes are added, with the different classes ordered from the highest to the lowest RFO, except for clear skies which is always last and displayed by the gray bar. The RFO of each class corresponds to the difference between cumulative RFO values at the right and left edge of the bar (i.e, width of the bar) representing the class. These global RFOs of each CVS class are also provided in the second column of Table 2. Note that the bars occupy the standard layers appropriate for each CVS class, in order to provide appropriate visualization. The bars are wider and connect across layers for contiguous classes (H×M, M×L, H×M×L).

The two most frequent CVS classes represent single-layer (according to our convention, i.e., confined to only one standard layer) cloud configurations: first is CVS="L" which occurs 26% of the time, followed by CVS="H" which occurs about half as often, with a 13.3 % frequency. The remaining single-layer CVS class, CVS="M" is far less frequent and occurs only 3.2% of the time making it the 6th most frequent CVS class. From the two-layer CVS classes with distinct

cloud layers, CVS=”HL” is the most frequent (~10% RFO, third overall), followed by CVS=”HM” (3%) and then CVS=”ML” (~2%), while of the two-layer CVS classes with contiguous cloud layers, CVS=”M×L” is slightly more frequent (3.5%) than CVS=”H×M” (2.9%). When all three standard layers are occupied by clouds, the one with contiguous clouds (as defined in our overlap model) CVS=”H×M×L” is far more frequent (fourth overall in frequency, RFO=9.5%) than the one with intervening clear skies between the layers, CVS=”HML”, which is the most rare CVS class with RFO=1.4%. Finally, clear skies happen ~25% of the time.

These results support the attention that single-layer “low” and “high” clouds (i.e., our CVS=”L” and CVS=”H”) have previously received in radiation budget studies as cloud configurations with potentially high SW CRE and low LW CRE contributions at the TOA and vice-versa [e.g., *Hartmann et al. 1992*]. This will be more precisely quantified here later. Not only are the CREs at the two distinct parts of the spectrum very different (*H* clouds are usually optically thin, producing small SW CRE), but the combined occurrence of these two single-layer CVS classes reaches 52.7% (=39.3/(1-0.254)) of all cloudy cases. *H* clouds overlapping *L* clouds is the third most frequent cloud configuration and has received attention before [*Yuan and Oreopoulos 2013*]. Mid-level clouds are also not as rare as commonly believed: they are quite rare globally as single-layer entities (CVS=”M” has RFO=3.2%), but can be frequent locally and as part of cloud configurations where they are not connected to clouds in the other two standard layers (according to our convention), namely in CVS classes “ML”, “HM”, and “HML”: when all these classes are considered collectively (along with CVS=“M”) “isolated” *M* clouds occur about ~10% of the time (~13% of cloudy skies). Note that this estimate may deviate

substantially from others that use only cloud top height (within a wide range of values) to determine presence of *M* clouds [e.g., *Zhang et al. 2010*].

In the following two sections we will examine how much variability is embedded in these annually-averaged global results. Specifically, we will examine daytime-nighttime differences, land-ocean differences, as well as the seasonal cycle of the zonal RFO distribution of the four most prominent CVS classes.

3.2 Daytime-Nighttime differences

Similar to Fig. 3, we now show two panels (Fig. 4a and 4b) of CVS class RFO frequency, but now composited separately from ascending (daytime) and descending (nighttime) observations by the two observational platforms. See also third and fourth column of Table 2 for exact values.

The frequency of clear-skies is larger during daytime compared to nighttime (27.4% vs 23.3%) and the ordering of CVS classes is also different although it must be noted that relatively small changes in the absolute frequency are sufficient to change the ordering. The largest absolute difference occurs for CVS=”HL”, with the daytime RFO dropping to 8.7% and making this CVS class slightly less frequent than CVS=”H×M×L”. Since single-layer *L* clouds (CVS=”L”) are actually slightly more numerous for daytime (26.4% vs 25.7%), broadly consistent with *Chepfer et al.* [2010] the reduction in CVS=”HL” probably comes mostly from *H* clouds (additional evidence is CVS=”H” having RFO=12.7% for daytime vs 13.9% for nighttime). Detection of the thinner of the *H* clouds may be affected by the varying quality between daytime and nighttime observations– daytime is noisier because of the presence of natural illumination, see *Nazaryan et al.* [2008]; *Chepfer et al.* [2010]. Indeed, the larger clear sky fraction of daytime observations

seems to be coming from fewer *H* clouds (note that all CVS classes involving *H* clouds have lower RFO in daytime compared to nighttime). When RFOs are normalized to represent percentages of cloudy-skies rather than all-skies, then we see that CVS=”L” is even more prevalent during daytime (RFO=36.4% vs 33.5%). The four most prevalent CVS classes represent 78.5% of clouds during daytime and 78.2% during nighttime, indicating that almost all of the decrease in the occurrence of clear skies during nighttime comes from cloud fraction increases by CVS=”H”, CVS=”HL” and CVS=”H×M×L”.

For daytime, we can compare our overall percentage of multi-layer occurrences relative to all clouds with that derived from MODIS-Aqua using appropriate information contained in the Level-3 dataset. Specifically, the CF corresponding to clouds on which successful optical property retrievals were performed and which were identified as multi-layer (Wind et al. 2010), can be divided by the CF of all successful retrievals. The global MODIS value of this ratio for our analysis period is ~16%. This is below the combined RFO of ~20% (relative to cloudy skies) of the “HL”, “HM”, “ML”, and “HML” CVS classes during daytime even though these do not include all multi-layer clouds (our simplified scheme reduces the near-contiguous cases to single-layer or contiguous). It is also below the 25% relative multi-layer occurrence obtained by Wang et al. (2016) from MODIS Level-2 data; the discrepancy between the two MODIS values may be due to one of the multi-layer tests being omitted in Level-3 aggregation (Platnick et al. 2016).

3.3 Land-Ocean differences

Our exploration of the variability of global CVS continues with an investigation of contrasts between oceanic and continental clouds. We use the land-ocean-coast mask included in the 2B-

GEOPROF-LIDAR product [*Mace and Zhang 2014*] for this exercise, with coastal profiles excluded.

The two panels of Fig 5 (and the fifth and sixth column of Table 2) reveal that there are very prominent differences between land and ocean. First of all, oceans are much cloudier according to 2B-CLDCLASS-LIDAR with 79.2% global mean CF dwarfing the 63.5% global mean CF of land, as found by *Chepfer et al.* [2010] and consistent with previous climatologies from entirely different types of measurements [e.g., MODIS, *King et al. 2013*]. Second, one sees that the dominance of CVS=”L” comes from the ocean where this CVS class occurs almost three times as often as land. Actually, over land CVS=”L” ceases to be the leading CVS as it is superseded by CVS=”H”. If one considers the fraction of these two CVS classes relative to the total amount of clouds in ocean and land, CVS=”L” represents 40.5% of oceanic clouds and 17.8% of continental clouds, while the figures for CVS=”H” are 15.2% and 26.0%, indicating that most of the overall reduction of land CF comes from CVS=”L” and that CVS=”H” does not nearly compensate, even if in relative terms it occurs almost twice as often over land than ocean when cloudy conditions exist. The other major contributor to the more extensive oceanic cloudiness is CVS=”HL” which forms more than twice as often over ocean (somewhat less as a fraction of cloudy only cases). Other notable land-ocean contrasts are CVS=”M” being mainly a continental CVS, ranking fourth in strength among its land brethren, while its ocean counterpart is the second rarest CVS; and CVS=”H×M×L” ranking fourth over ocean while being third in strength over land despite the two RFOs having the same contribution to the overall cloudiness of oceans and lands.

3.4 Seasonal and geographical variability of major cloud vertical structures

Our analysis so far has shown that the most dominant CVS classes are CVS=”L”, CVS=”H”, CVS=”HL” and CVS=”H×M×L” with the last two having very similar RFOs. These four CVS classes combine for a total RFO of 58.4% which stands for 78.3% of cloud skies. We therefore focus only on these dominant CVS classes to examine joint seasonal and geographical variability of cloud vertical configurations. Fig. 6 shows the results in the form of month-by-month variations of the multi-annual zonal monthly means. These plots then inform us on whether these CVS classes exhibit maxima or minima of occurrence at specific latitudes and parts of the year.

CVS=”L” (Fig 6a), our most frequent CVS class, appears to be much more prominent in the Southern Hemisphere (SH). This should come as no surprise as we have previously seen that this CVS class is mostly oceanic in nature. A prominent peak can be seen in the subtropics consistent with the presence of marine stratocumulus at those latitudes. The peak occurs during July-August-September-October in agreement with previous studies documenting the seasonal variability of these types of clouds [*Oreopoulos and Davies 1993*; *Norris and Leovy 1994*]. A second subtropical peak, somewhat more poleward happens during SH summer and is probably associated with the weaker parts of mid-latitude storms intruding northward. Another more typical SH mid-latitude peak associated with storms is found further to the south during the summer months. The Northern Hemisphere (NH) has two peaks for this CVS class near polar latitudes during the spring and autumn months.

Panel (b) of Fig. 6 reveals that CVS=”H” is mainly a tropical CVS that peaks slightly north of the equator during the April to June period. Something similar is observed for CVS=”HL” (Fig. 6c) which actually has a peak at almost in the same part of the graph (i.e., same latitude and

time of the year). Both of these CVS classes seem therefore to be closely associated with tropical convection. On the other hand, CVS="H×M×L" is associated not only with convection (tropical peak clearly seen in Fig. 6d), but also with mid-latitude storms at both hemispheres, especially during the winter months, although the largest RFO in the SH actually occurs during the spring. Note that many of the near-peak RFOs at both hemispheres occur at locations and times of the year with no solar illumination, so comparisons with cloud observations from reflected solar signals are not possible.

3.4 Radiative Effects of Cloud Vertical Structures

Given the strong dependence of thermal emission on temperature, it is obvious that the vertical arrangement of clouds within the atmosphere must have a large effect on the longwave flux at the top and bottom of the atmospheric column. But as we will see shortly, the shortwave radiative effect has also a strong dependence on CVS class. This is because the various classes are associated with systematically different total opacities stemming from differences in vertical extent and the tendency of clouds encountered in the three standard layers to exhibit different physical and optical properties.

Fig. 7 gives the global radiative influence of CVS classes according to compositing of 2B-FLHXR-LIDAR data [*L'Ecuyer et al. 2008; Henderson et al. 2013; Matus and L'Ecuyer 2017*]. For every profile in 2B-CLDCLASS-LIDAR that was assigned a CVS class we extract the radiative fluxes from 2B-FLHXR-LIDAR and calculate area-weighted means per CVS class. What Fig. 7 specifically shows is the TOA and BOA mean CREs (calculated from net=down-up fluxes) for each CVS class for both SW (red bars) and LW (blue bars). Also shown in the middle of the graph

is the total atmospheric CRE calculated as the difference between the TOA total (=SW+LW) and BOA total CREs.

Figure 7 immediately reveals the wide range of SW and LW CRE values at both the TOA and BOA. While the SW CRE varies greatly among the CVS classes, it is at the same time apparent that the TOA and BOA (surface) components have rather similar values. BOA values are slightly larger because of clouds providing a small amount of additional absorption to the atmospheric column (the additional absorption by the cloud particles exceeds overall the reduced water vapor absorption at the lower atmosphere due to inhibited solar irradiance). The largest SW CRE corresponds not surprisingly to the CVS structure expected to contain most often the optically thickest clouds, CVS=”H×M×L”. Next comes CVS=”HML” which also contains clouds in all three standard layers, and is therefore also likely to be opaque.

Contrary to the SW, the LW CRE values can be vastly different at TOA and BOA depending on CVS class. For example, CVS=”L” produces little LW TOA CRE because low clouds change the effective height of emission to space very little compared to a clear atmosphere, but affect greatly the LW flux toward the surface because these clouds greatly increase the infrared opacity of the lower atmosphere. On the other hand, CVS classes containing *H* clouds have high LW TOA CRE, but the magnitude of their BOA CRE is modulated by the co-occurrence of clouds in other standard layers; contrast for example CVS=”H” with CVS=”HML”.

The dependence of total atmospheric CRE on CVS class is also very intriguing. This radiative quantity tells us whether clouds provide an overall cooling (negative CRE value) or warming (positive CRE value) to the atmospheric column as a whole. The middle part of Fig. 7 reveals which CVS classes enhance the radiative cooling of the clear atmosphere (blue shade)

and which work alongside latent heating due to condensation to mitigate it (red shade). We see that only three CVS classes are radiative coolers and all of them contain *L* clouds, with CVS="L" providing the strongest cooling. Adding *M* clouds reduces the cooling, and actually CVS="M" achieves an almost exact balance between radiative cooling and warming for the atmosphere as a whole, and is therefore not assigned a color shade; cooling and warming may nevertheless occur at different altitudes. For a CVS class to be a radiative warmer of the atmosphere it must have *H* clouds. When *L* clouds co-occur with *H* clouds, the radiative heating generally weakens: from the six CVS classes that are radiative warmers, CVS="HL" and CVS="HML" are the weakest. The exception is our most vertically extensive CVS class, CVS="H×M×L", which is the second strongest radiative warmer. Note that CVS="H" has neither the strongest LW TOA CRE, nor the strongest ATM total CRE. Additional cloud opacity in the form of *M* clouds is needed to make these CREs stronger, with the largest magnitudes achieved by CVS="H×M".

While Fig. 7 shows the mean magnitude of the radiative impact of the different CVS classes when they occur, the overall radiative importance of each CVS class depends on its frequency of occurrence. We try to convey this in Table 3 which shows the percentage radiative contribution of each CVS class to the global CRE for four CRE components, calculated as the ratio of the area-weighted sum of all CRE values for the particular CVS class to the area-weighted sum of all valid CRE values regardless of CVS class:

$$contribution(\%)_CRE_CVS_j = \frac{\sum_{i=1}^{N_j} w_i CRE_i}{\sum_{k=1}^{10} \sum_{i=1}^{N_k} w_i CRE_i} \times 100 \qquad (2)$$

N_j is the number of profiles corresponding to CVS_j, N_k is the number of profiles corresponding to CVS_k, and w_i is the weight (=cosine of latitude) for profile i.

The contribution to the total ATM CRE is shown differently because its sum over all CVS classes is a small value due to cancellations between positive and negative CREs (specifically, it is 6.3 Wm^{-2}, close to the *Henderson et al. 2013* and *Matus and L'Ecuyer 2017*); instead of percentages we show the contribution in Wm^{-2} of each CVS class calculated as the ratio of the area-weighted sum of total ATM CRE values, for the CVS class of interest, to the sum of area weights of all CVS class occurrences:

$$contribution_CRE_{TOT}^{ATM}_CVS_j = \frac{\sum_{i=1}^{N_j} w_i CRE_{iTOT}^{ATM}}{\sum_{k=1}^{10}\sum_{i=1}^{N_k} w_i} \quad (3)$$

In other words, the numbers in the last column of Table 3 derived from Eq. (3) add up to 6.3 Wm^{-2}. The results from eq. (3) are slightly different from those obtained by multiplying the area-weighted mean total ATM CRE of a CVS class (Fig. 7) with its area-weighted RFO (2nd column of Table 3).

For the SW CRE, we see (Table 3) that TOA and BOA are virtually the same because the mean values differ by a small amount that remains relatively constant. CVS="L" rises to the top as the strongest SW CRE contributor because of its large RFO, even though its mean CRE values are nowhere near the strongest. CVS="H×M×L" is actually the CVS class with the strongest mean SW CRE values, but comes second because it ranks only fourth in RFO. In the LW, we saw earlier the TOA and BOA CRE values are very different and this carries to the contributions. At TOA, CVS="H×M×L" ranks as the strongest contributor at ~31%, combining the second strongest mean value with the fourth largest RFO. CVS="H×M" has a slightly stronger mean value, but because its RFO is only ~3%, it reaches only about a third the contribution of CVS="H×M×L". While *L* clouds are often ignored in LW CRE discussions because we usually focus on radiative

impacts at TOA, Table 3 makes clear that they are (at least in the form of CVS=”L”) by far the strongest contributor to surface thermal infrared warming with ~40% contribution. This CVS class while not having the strongest mean value of LW BOA CRE, occurs so often that in the end assumes an extremely important role in the LW surface radiation budget.

Finally, the great role of RFO in assessing radiative importance reveals itself conspicuously for total ATM CRE (Table 3). The major contributors are three of the four CVS classes with the highest RFOs, namely CVS=”L”, CVS=”H”, and CVS=”H×M×L”. On the flipside, a high RFO by itself does not make a CVS class a large contributor: CVS=”HL” is third most frequent, but the mean total ATM CRE is only ~5 Wm^{-2}, making it contribute only ~0.6 Wm^{-2} to the global value which may seem like a respectable ~10% contribution, until we realize that it represents only ~4% of the overall warming contribution (the sum of positive total CRE ATM values).

4. Cloud Vertical Structures of MODIS Cloud Regimes

The analysis shown here is in the same vein as that by *Tselioudis et al.* [*2013*] for ISCCP Weather States. Although derived using a different methodology and dataset, our CVS classes are the same as in that paper and serve the same ultimate goal: to further understand and validate the robustness and meaningfulness of cloud systems classified into regimes by grouping together similar co-variations of cloud properties derived from passive satellite observations.

4.1 Nominal MODIS CRs

Fig. 8 shows the breakdown of each of O16’s MODIS CRs by CVS class. To achieve the spatiotemporal matching necessary to perform the analysis only Aqua CR occurrences and

daytime 2B-CLDCLASS-LIDAR data are used (since CRs can be determined only during daytime). Previous interpretations of the nature of MODIS CRs based on centroid appearance and the most prevalent location of CR members (see Table 1) are largely consistent with the composition by CVS class as we detail below.

CR1 has been interpreted as being mainly a tropical regime with the largest fraction of cirrus clouds, but also many vertically developed clouds from convective activity. The CVS breakdown shows CVS="H" dominating (RFO~50%) followed by CVS="HL"; these two classes make up about 77% of CR1. If CVS="H×M×L" is used in this case as a surrogate of deep convective towers, then they occur about 13% of the time within CR1, and it certainly appears that they are accompanied by plentiful cirrus anvils (CVS="H"). CR2 was described in O16 as containing tropical and frontal convection, and the breakdown by CVS class seems to confirm this with CVS="H×M×L" RFO exceeding 60%. While CVS="H×M" is not very important globally, it is a significant contributor to CR2 with an RFO of ~13%. As with CR1, almost all of CR2 consists of CVS classes containing *H* clouds. CR3 shares features with both CR1 and CR2, having CVS="H" and CVS="HL" as the dominant class (similar to CR1), but also having substantial amounts of CVS="H×M×L" and CVS="H×M", similar to CR2.

CR4 and CR5 were previously linked to mid-latitude storms, with CR4 containing more optically thick clouds, something that is reflected in the CVS class breakdown with ~20% higher RFO in CVS="H×M×L" than CR5. While CR4 has virtually no CVS="H", for CR5 this class is the third most frequent, and a likely a reason for the lower mean COT (Table 1), along with CVS="H×M" which is rarer in CR4. Note also that CR4 and CR5 are the regimes with the highest RFO of the very rare globally CVS="HML" which occurs almost exclusively within CR2-5. The

centroid of CR6 (Fig. 2) has prompted us to identify this regime as the most “mid-level cloud” regime because of the histogram peak within the 440-680 hPa standard layer. Active observations confirm this, with the globally rare CVS=”M” having an RFO of ~16% within that CR (incidentally, CR4 and CR5 also have substantial amounts of this CVS class). CR6 also has high RFOs for the two other classes with unobscured (from space) *M* clouds, CVS=”M×L” and CVS=”ML”, with the former being actually the most dominant CVS class within CR6.

Moving on now to CRs dominated by liquid clouds, we see an abrupt transition in CVS morphology from CR6 to CR7. CR7 is dominated by CVS=”L” and the RFO of this class (~70%) remains approximately the same in CR8 and CR9 as well. So, these three regimes are largely single-layer regimes. CVS=”L” RFO progressively drops in CR10 (still about 60% of the time), CR11 and CR12, and these reductions accompany an overall decrease in CF. All regimes from CR7 to CR11 have CVS=”HL” as the second most important CVS class indicating that *H* clouds over *L* clouds is a rather frequent overlap configuration that has justifiably received attention in the past [*Yuan and Oreopoulos* 2013]. The most frequent regime with the lowest CF, CR12, is quite complex in terms of CVS class breakdown. It seems to consist of both CVS=”H” and CVS=”L”, but also their combination, CVS=”HL”. It will be discussed further in the next subsection.

Finally, it is important to point out that the CF of CR10, CR11 and CR12 differs considerably between MODIS and CloudSat/CALIPSO, with the difference being quite dramatic for CR12. It appears then that CR12 contains numerous small and optically thin elements that remain undetected by MODIS, but produce strong enough backscatter signals for CALIPSO’S CALIOP lidar to discern from the atmospheric background [*Wang et al.* 2016].

4.2 MODIS subregimes

While by construction a CR represents an ensemble of joint CTP-COT histograms that are alike, individual member histograms belonging to the same CR may still be quite different. The fact that they were assigned to the same CR simply means that they were even more distinct from histograms that ended up assigned to other CRs. Within the set of histograms that make up a CR we can identify subsets whose members are *even more alike*. We call the ensemble means of these subsets "subregimes" [*Mason et al.* 2014]. Different options to define subregimes are available. Here we adopt the method previously used by *Leinonen et al.* [2016] which is based on quartiles of Euclidean Distance (ED) from the CR centroid as described in subsection 2.3. The objective in this subsection is to compare the CVS composition of subregimes for the four CRs exhibiting the most dramatic CVS contrast between 1q and 3q subregimes (the 2q subregime as an ensemble average of histograms with close-to-median EDs is resembling closely its centroid). The regimes selected for the analysis shown in Fig. 9 are CR1, CR5, CR6, and CR12.

Our simple subregime identification procedure produces a $CR1_{3q}$ with a large RFO of CVS="H×M×L" which seems to have grown at the expense of CVS="H". $CR1_{1q}$ has more CVS="H" and less CVS="H×M×L" than the centroid (Fig. 8). So, our simple subregime definition has sufficient skill to separate the histograms containing the most convective elements of the regime. The two 3q and 1q subregimes of CR5 are also very different with regard to their vertically extensive clouds represented by CVS="H×M×L". Moreover, $CR5_{1q}$ has CVS="H" as the second most frequent class, while for $CR5_{3q}$ this class is encountered much less (fourth overall). In general, the RFOs of different CVS classes are more evenly distributed in $CR5_{1q}$: notice that it takes four CVS classes to reach a cumulative RFO of ~63% for $CR5_{1q}$ while it takes only two for

$CR5_{3q}$. The breakdown of CR6 into subregimes reveals that more CVS=”M” comes from the histograms with smaller Euclidean distances from the centroid (1q) (and also smaller overall CFs). $CR6_{1q}$ has fewer occurrences of all other major CVS classes within this regime (CVS=”L”, ”M×L”, ”H×M×L”).

The breakdown into subregimes and reconstruction of CVS partitioning becomes even most interesting for CR12 (Fig. 9d). The two subregimes are completely different in terms of cloud fraction, with $CR12_{1q}$ made almost exclusively by low fraction (RFO) single layer clouds CVS=”L”, complemented by CVS=”H”. The much more cloudy $CR12_{3q}$, on the other hand, has in addition to those two CVS classes also substantial amounts of CVS=”HL” and CVS=”H×M×L”. The presence of the latter class, as well of CVS=”H×M” explains $CR12_{3q}$’s considerable precipitation production (according to our own analysis not shown here) and justifies the inclusion of the parent CR12 in the group of CRs for which invigoration is investigated [*Oreopoulos et al. 2017*].

5. Summary and Conclusions

We have performed a comprehensive analysis of cloud vertical structure (CVS) at global scales using a product (2B-CLDCLASS-LIDAR) that combines observations from active space-based sensors, namely the CALIOP lidar aboard the CALIPSO satellite and the CPR radar aboard the CloudSat satellite. These satellites and instruments fly in formation as part of the A-Train constellation and therefore make contemporaneous collocated observations. Moreover, their measurements can also be collocated with those by the MODIS instrument aboard the Aqua satellite, also part of the A-Train, something we also take advantage of in this study.

We have attempted to capture the richness of CVS with minimal sacrifice in information content, by reducing complex cloud configurations into a few intuitive vertical arrangements (CVS “classes”) where clouds in a particular vertical profile occupy either one, two or three standard vertical layers. We found that CVS classes previously defined by *Tselioudis et al.* [*2013*] are suitable for this purpose, even though a different dataset and methodology was used to derive them in that effort.

Our study makes a significant contribution to the knowledge of global cloudiness. We determined which cloud vertical configurations are more frequent at global scales (single layer low, CVS=”L”, and high clouds, CVS=”H” represent ~53% of cloudy skies) and whether the frequencies of the CVS classes differ substantially when examined separately for daytime versus nighttime (~4% more clouds overall in the latter case, but with the occurrence order of the CVS classes affected only in minor ways), and land versus ocean (the dominance of CVS=”L” was found to overwhelmingly come from ocean occurrences). The seasonal and geographical variations of the four most dominant CVS classes are substantial, with easily discernible patterns consistent with our understanding of global circulation and weather systems.

We also have added to our understanding of how different cloud systems affect the radiation budget, previously examined in terms of cloud type [*Hartmann et al.* 1992; Chen et al. 2000], cloud phase [Matus and L'Ecuyer 2017], and cloud regime [*Haynes et al.* 2011; *Oreopoulos and Rossow* 2011; *Tselioudis et al. 2013*; *Oreopoulos et al.* 2014; *Oreopoulos et al.* 2016]. This study adds a piece to the puzzle by providing cloud radiative impact based on vertical configuration classification. We show which CVS classes have strong, moderate, or weak impacts on TOA, surface and atmospheric radiation budgets using as criteria either mean

instantaneous magnitudes or overall contributions. We found, for example, that single-layer low clouds (CVS=”L”) dominate planetary and atmospheric cooling, and thermal infrared surface warming; the vertically extensive cloud configuration (CVS=”H×M×L”), despite being only the fourth most frequent CVS class, is either first or second in radiative importance for both the solar and the thermal infrared regardless of whether one focuses on the planet as a whole (TOA), the surface, or the atmosphere.

We also looked closely at how passive and active cloud observations compare. Previously defined cloud regimes derived from MODIS cloud optical thickness and cloud top pressure co-variations were probed in terms of their internal distribution of CVS classes and were shown to have considerable amounts of internal variability. Reassuringly, our analysis also revealed that the interpretations of the nature of the MODIS regimes were largely on target, a conclusion that complements the findings of *Leinonen et al.* [2016] which were based exclusively on comparisons with CloudSat CPR reflectivities.

Although the path to replicate our CVS classification in AGCMs is not obvious, and may require more sophisticated subcolumn cloud generators than currently available in order to create credible subgrid cloud variability, we hope that cloud validation in this class of models will now have an additional aspect of cloud morphology to consider.

Acknowledgements

Funding by NASA’s “The Science of Terra and Aqua” program is gratefully acknowledged. The MODIS cloud regimes used in this study can be provided by the lead author upon request. Other MODIS datasets can be obtained at https://ladsweb.modaps.eosdis.nasa.gov/search/.

CloudSat datasets can be obtained at http://www.cloudsat.cira.colostate.edu. We thank our colleagues Kerry Meyer and Steven. E. Platnick for helpful discussions about MODIS products.

Appendix

We provide here details of how the cloud vertical stratification extracted from 2B-CLDCLASS-LIDAR was condensed into the 10 cloudy CVS classes of *Tselioudis et al.* [*2013*].

(1) *Single contiguous cloud.* When a single contiguous cloud is identified in 2B-CLDCLASS-LIDAR (47.4% of available profiles, Fig A1), possible scenarios are [CTP=Cloud Top Pressure; CBP=Cloud Bottom Pressure]:

a. The cloud is confined to one of the three standard layers: if [CTP and CBP ≤ 440 hPa] then CVS =”H”; if [CTP and CBP > 440 hPa] and [CTP and CBP ≤ 680 hPa] then CVS=”M”; if [CTP and CBP > 680 hPa] then CVS=”L” (see Fig. A1, case (a)).

b. The cloud spans two standard layers (Fig. A1, case (b)): there are two possibilities, CTP ≤ 440 hPa and 440 hPa < CBP ≤ 680 hPa in which case the default is CVS=”H×M”; and 680 hPa <CTP ≤ 440 hPa and CBP > 680 hPa in which case the default is CVS=“M×L”. The default case applies when the cloud is “thick”, defined as CBP-CTP ≥ 200 hPa (note that our analysis examines cloud thickness only when the cloud spans two or three standard layers, i.e., crosses standard layer boundaries). Otherwise (CBP-CTP < 200 hPa, cloud is thin), the CVS =”H×M” class can revert to either CVS=”H” or CVS=”M”, while the CVS=“M×L” can revert to either CVS=”M” or CVS=”L”. This re-classification to a single-layer CVS category depends on the pressure of the cloud’s geometric center location determined by logarithmic averaging of CTP and CBP. If the center location falls within the top standard layer then CVS=”H”, if it falls within the middle standard layer then CVS=”M”, and if it falls within the bottom standard layer then CVS=”L”. The re-assignment of “thin” clouds

crossing standard layer boundaries to a CVS class representing a single cloud layer deviates from the ISCCP approach of assigning clouds to standard layers according to CTP. Now that we have additional information on CBP in our disposal, our philosophy is to make the assignment based on where the bulk of the "thin" cloud resides.

c. If the cloud spans all three standard layers (Fig. A1, case (c)), i.e., [CTP ≤ 440 hPa and CBP> 680 hPa] and is "thick", defined as CBP-CTP ≥ 440 hPa (=pressure thickness of the standard middle layer + 200 hPa as before) then the cloud is assigned to the default CVS="H×M×L" category. When the cloud is "thin", i.e., CBP-CTP < 440 hPa, then its presence in one or two of the standard layers may be small, so that CVS="H×M×L" reverts to CVS="H×M" when CTP < 340 (=440-100) hPa (not much cloud resides in the bottom standard layer), to CVS="M×L" when CBP > 780 (=680+100) hPa (not much cloud resides in the top standard layer), and to CVS="M" when the cloud is "thin" and none of the other conditions apply.

(2) *Two distinct cloud layers.* When two distinct layers of cloud are identified in 2B-CLDCLASS-LIDAR (20.5% of profiles, Figs. A2, A3), possible scenarios are:

a. The top and bottom of *both* cloud layers are confined within one of the standard layers. Then the two cloud layers within the standard layer are considered single layer clouds for our purposes, resulting in one of CVS="H", CVS="M", CVS="L" (Fig. A2, case (a)).

b. Each of the two cloud layers is confined to a *different* standard layer. The CVS class is then one of the three possible classes that indicate separate (non-contiguous) cloud

layers each belonging to a different cloud category. Namely, CVS=”HM”, CVS=”HL”, or CVS=”ML” (Fig. A2, case (b)).

c. One of the cloud layers spans two standard layers while the other is confined to a single standard layer. Now there are two possibilities:

   i. The two cloud layers have a common standard layer, for example the topmost cloud is “H” while the cloud below is “H×M” (abbreviated here as [H, H×M]); if the “H×M” is thick (CBP-CTP ≥ 200 hPa) then it is considered merged with the “H” cloud resulting in CVS=“H×M”. On the other hand, if the “H×M” layer is “thin”, then we calculate the location of the cloud center as before by taking the logarithmic average of its CTP and CBP, and reduce it to a cloud that is confined to a single standard layer, i.e, either “H” or “M”; in the former case, CVS=”H” (cloud merging), while in the latter case CVS=”HM” (Fig. A2, case (c(i))). Other possible cases (not illustrated) in this type of scenario are: [H×M,M] which can result in CVS=”H×M” when the highest cloud H×M is thick (merge with “M”), or CVS=”HM” or CVS=”M” for the cases of thin H×M clouds with different geometric centers; [M×L,L] similarly yields either CVS=”M×L” (thick M×L cloud) or CVS=”ML” or CVS=”L”; [M,M×L] yields either CVS= “M×L” (thick M×L cloud) or CVS=”ML” or CVS=”M”.

   ii. The cloud layers do not have a common standard layer: Two cases are now possible. One case is [H,M×L] which becomes CVS=”H×M×L” when the bottom M×L cloud is thick, or CVS=”HM” or CVS=”HL” when the bottom cloud is thin, depending on the standard layer its geometric center falls into

(Fig. A2, case (c(ii))); the other case is [H×M,L] (not illustrated) which yields either CVS=”H×M×L” (thick H×M cloud) or CVS=”HL” (thin H×M cloud whose center is in top standard layer) or CVS=”ML” (thin H×M cloud whose center is in middle standard layer) .

d. Each of the cloud layers spans two standard layers, namely [H×M, M×L] (Fig. A3, case (d)). If both layers are thick then CVS=”H×M×L”. If both layers are thin then we look at cloud center locations: if both fall in the middle standard layer then CVS=”M” or they can be in different standard layers, resulting in one of CVS=”HM”, CVS=”HL”, CVS=”ML”. If the H×M cloud is thick and the M×L cloud is thin then CVS=”H×M×L” when the center of the lower cloud is located within the lowest standard layer, while CVS=”H×M” when its center is located in the middle standard layer (cloud merging in both cases). If on the other hand the H×M cloud is thin and the M×L cloud is thick then the center location of the top cloud determines the final CVS outcome: CVS=”H×M×L” results when the center is in the topmost standard layer, while CVS= “M×L” when the center resides in the middle standard layer.

e. One of the cloud layers spans three standard layers while the other is confined to a single standard layer, namely the cloud configuration is either [H, H×M×L] (Fig. A3, case (e)) or [H×M×L, L] (not illustrated). In this case we examine the thickness of the H×M×L cloud layer using the 440 hPa threshold as before. For both configurations, when the H×M×L cloud layer is thick then CVS=”H×M×L”. If the H×M×L cloud is thin on the other hand we examine the center location according to the description in 1c and the cloud is reduced to either “M”, or “H×M”, or “M×L”. When these clouds are

combined with the H cloud of the [H, H×M×L] configuration, possible CVS outcomes are, respectively, CVS="HM", CVS="H×M", CVS="H×M×L" (Fig. A3, case (e)), while when they are combined with the L cloud of the [H×M×L, L] configuration, then one of CVS="ML", CVS="H×M×L", CVS="M×L" will be the final outcome (not shown).

(3) *Three distinct cloud layers.* When three distinct layers of clouds are identified in 2B-CLDCLASS-LIDAR (5.8% of profiles) there are 78 possible configurations for our simplified cloud overlap model, with broad scenarios being:

a. The top and bottom of *all three* cloud layers are confined within one of the standard layers. Then the three cloud layers within the standard layer are considered as a single layer (cloud merging), resulting in CVS="H", or CVS="M", or CVS="L" (Fig. A4, case (a)).

b. Each of the three cloud layers is confined to a *different* standard layer. Then CVS="HML" (Fig. A4, case (b)).

c. Two of the three cloud layers are confined within one standard layer while the third layer is confined to a *different* standard layer (Fig. A4, case(c)). Possible CVS outcomes in this case are: CVS="HM" for either two cloud layers in the top standard layer and one in the middle standard layer, or for one cloud layer in the top standard layer and two in the middle standard layer; CVS="HL" for either two cloud layers in the top standard layer and one in the bottom standard layer, or for one cloud layer in the top standard layer and two in the bottom standard layer; CVS="ML" for either two cloud layers in the middle standard layer and one in the bottom standard layer,

or for one cloud layer in the middle standard layer and two in the bottom standard layer.

d. One of the three cloud layers spans two or three standard layers (not illustrated). There are now too many scenarios to describe, but the gist is that to arrive at one of our 10 CVS classes we follow on the footsteps of what was done in our previous simpler configurations. Basically, we examine whether the cloud crossing standard layer boundaries is thick or thin and apply the logic described earlier. If the cloud crosses two boundaries (spans three standard layers) and is thick (≥ 440 hPa), then CVS="H×M×L"; if it's thin, it is reduced using the center location calculation described above to a cloud spanning two standard layers, and the eventual CVS outcome depends on whether this cloud shares a common standard layer with the remaining cloud layer.

e. Two of the three cloud layers span two standard layers. Again, there are numerous permutations, but the CVS assignment can be done using rules already established previously. CVS="H×M×L" is a frequent outcome, as expected, if both or even one of the clouds spanning the two standard layers is thick (≥ 200 hPa), depending also on the location of the other cloud layer. But CVS classes indicating non-contiguous clouds are also possible, especially when both cloud layers crossing standard layer boundaries are thin.

(4) *Four or more distinct cloud layers.* When four or more distinct cloud layers exist (only 0.9% of profiles), then we derive CVS classes only for the simpler cases where the cloud entities

do not cross standard layer boundaries, using the concepts and logic described above (0.4% of profiles).

Applying all the above assigns the vast majority of cloud vertical configurations in a given profile, with only a small fraction (0.5% of the overall cloudy columns) being too complex for CVS derivation, and therefore discarded.

List of Tables

Table 1. Brief description and globally-averaged properties of the 12 MODIS CRs introduced by *Oreopoulos et al.* [*2016*] and used in this study. The CF is weighted by area, so is slightly different from that of Fig. 2 which corresponds to the sum of the bin CFs within the centroids.

CR	Description	RFO (%)	CF (%)	Mean COT	Mean CTP (hPa)
CR1	Mostly tropical with a pronounced presence in the Pacific ocean, and elsewhere within the confines of ITCZ. Contains a lot of the tropical cirrus associated with convection, but also deeper convective clouds.	3.46	84.0	9.9	292
CR2	Contains most of the optically thickest and tallest clouds of all CRs; includes storm systems produced by tropical and frontal convection and has the highest CF of all regimes.	2.99	96.6	23.4	354
CR3	Tracks tightly the geographical pattern of CR2, but contains the thinner elements of storm activity.	5.02	89.0	7.7	369
CR4	Extratropical and dominated by alto- and nimbo- type clouds in higher latitude storm systems. More prevalent during the summer months.	3.77	92.5	25.8	477
CR5	Closely associated with CR4, but with fewer optically thick clouds and more prevalence during the winter months.	3.68	86.5	10.9	490
CR6	Contains proportionally the most mid-level clouds and also has some congestus, with strong land presence.	6.99	83.2	22.3	602
CR7	Mainly a high latitude CR of plentiful thick stratus over both land and ocean with small RFO and big CF.	2.44	95.7	26.8	721
CR8	Boundary layer regime with occurrence peaks in known marine stratocumulus areas, but additional presence in far southern oceans and northern lands.	4.92	86.7	12.9	738
CR9	Similar to CR8 in CF, but of a more marine character and with shallower and optically thinner clouds; presence also peaks in known marine stratocumulus areas.	7.62	91.1	13.9	821
CR10	Also as marine as CR9, but with lower CF indicating greater relative presence of broken stratocumulus and shallow cumulus.	7.28	68.3	6.6	817
CR11	Even more broken stratocumulus and shallow cumulus than CR10, with small optical thicknesses and low cloud fractions; almost exclusively oceanic with negligible presence in high latitudes.	10.36	50.3	4.6	836
CR12	Comprises all 2D histograms with no characteristic shape, or histograms with a dipole pattern where high clouds overlap low clouds; has the highest global RFO and smallest CF, and except the nearly always overcast far southern oceans, is nearly omnipresent.	41.47	29.3	11.9	705

Table 2. Area-weighted Relative Frequency of Occurrence (RFO, in %) of the different CVS classes, ordered from highest to lowest by the global RFO of each class (second column). The remaining columns show special situations, namely global RFOs for daytime only, nighttime only, ocean only, and land only observations.

CVS class	Daily	Daytime	Nighttime	Ocean	Land
L	26.0	26.4	25.7	32.1	11.3
H	13.3	12.7	13.9	12.0	16.5
HL	9.7	8.7	10.6	11.4	5.5
H×M×L	9.5	9.2	9.8	10.0	8.1
M×L	3.5	3.5	3.5	3.6	3.2
M	3.2	3.3	3.2	1.9	6.6
HM	3.0	2.6	3.5	2.1	5.3
H×M	2.9	2.9	2.9	2.4	4.2
ML	2.2	2.2	2.1	2.3	1.7
HML	1.4	1.2	1.5	1.4	1.2
Clear	25.4	27.4	23.3	20.8	36.5

Table 3. Percentage contributions of the different CVS classes to different CRE components (columns SWTOA, LWTOA, SWBOA, LWBOA). The last column represents the Wm^{-2} contribution of each CVS class (Eq. 3) to the global total ATM CRE of 6.3 Wm^{-2}.

CVS class	RFO	SWTOA	LWTOA	SWBOA	LWBOA	totATM
L	26.0	31.2	9.9	31.1	39.7	-8.9
H	13.3	4.2	20.1	4.3	4.0	6.2
HL	9.7	10.3	10.4	10.3	10.3	0.6
H×M×L	9.5	26.2	31.3	26.4	18.7	6.3
M×L	3.5	7.5	4.8	7.6	8.7	-0.9
M	3.2	4.3	4.0	4.2	4.6	0.0
HM	3.0	4.4	5.2	4.2	3.1	0.9
H×M	2.9	5.0	9.7	5.1	4.4	2.3
ML	2.2	4.2	2.4	4.1	4.3	-0.5
HML	1.4	2.8	2.2	2.7	2.1	0.2

List of Figures

Figure 1. Graphical illustration of our 10 CVS classes based on the details of the vertical stratification of clouds in the three standard atmospheric layers.

Figure 2. The centroids (average joint histograms) that define the MODIS Global Cloud Regimes used in one of the main components of this study. These regimes were introduced by O16. Above each panel we show the global averages of Relative Frequency of Occurrence (RFO, in %, as defined in O16) and Cloud Fraction (CF, in %).

Figure 3. Area-weighted RFOs of the various CVS classes plotted in cumulative form using bars that occupy the standard layers relevant to each class and have widths corresponding to each CVS class RFO in % (values also provided in second column of Table 2). The CVS classes are ordered from the largest to the smallest RFO. The gray bar indicates clear skies.

Figure 4. As in Fig. 3, but now separately for daytime (ascending node, panel (a)) and nighttime (descending node, panel (b)) conditions. Individual CVS class RFOs are also provided in the third and fourth column of Table 2.

Figure 5. As in Fig. 4, but now separately for oceanic (panel (a)) and continental (panel (b)) conditions. Individual CVS class RFOs are also provided in the fifth and sixth column of Table 2.

Figure 6. Seasonal (month-by-month) variations of the zonal RFO of the four most dominant CVS classes. (a) CVS=”L”; (b) CVS=”H”; (c) CVS=”HL”; (d) CVS=”H×M×L”.

Figure 7. Graphical illustration of CRE strength for the various CVS classes. The graph shows the area-weighted mean SW and LW CRE at both TOA and BOA, as well as the total (=SW+LW) CRE in the atmosphere (middle of graph), a measure of heating or cooling induced by clouds in the atmospheric column. CRE composite values come from collocated 2B-FLXHR-LIDAR data.

Figure 8. CVS RFOs within each of the MODIS CRs of O16. Conventions are the same as in Fig. 3. To achieve spatiotemporal matching, only Aqua CR occurrences and daytime CVS data were used.

Figure 9. As Fig. 8, but for the 1q and 3q subregimes (see text) of CR1(a), CR5(b), CR6(c), and CR12(d).

Figure A1. Examples of CVS class assignment for the case of a single contiguous cloud layer.

Figure A2. Select examples of CVS class assignment for the case of two distinct (non-contiguous) cloud layers.

Figure A3. Additional examples of CVS class assignment for the case two distinct (non-contiguous) cloud layers.

Figure A4. Select examples of CVS class assignment for the case of three distinct (non-contiguous) cloud layers.

References

Barker, H. W. (2008b), Overlap of fractional cloud for radiation calculation in GCMs: A global analysis using CloudSat and CALIPSO data, *J. Geophys. Res.*, **113**, D00A01, doi:10.1029/2007JD009677.

Chang, F.-L., and Z. Li (2005a), A new method for detection of cirrus-overlapping-water clouds and determination of their optical properties, *J. Atmos. Sci.*, **62**, 3993–4009.

Chang, F.-L., and Z. Li (2005b), A near-global climatology of single-layer and overlapped clouds and their optical properties retrieved from Terra/MODIS data using a new algorithm, *J. Clim.*, **18**, 4752–4771.

Chen, T., W. B. Rossow, and Y. C. Zhang (2000), Radiative effects of cloud-type variations, *J. Climate*, **13**, 264–286, doi:10.1175/1520-0442(2000)013<0264:REOCTV>2.0.CO;2.

Chepfer, H., S. Bony, D. Winker, G. Cesana, J. L. Dufresne, P. Minnis, C. J. Stubenrauch, and S. Zeng (2010), The GCM-Oriented CALIPSO Cloud Product (CALIPSO-GOCCP), *J. Geophys. Res.*, **115**, D00H16, doi:10.1029/2009JD012251.

Hartmann, D. L., M. E. Ockert-Bell, and M. L. Michelsen (1992), The effect of cloud type on Earth's energy balance: Global analysis, *J. Clim.,* **5**, 1281–1304.

Haynes, J., C. Jakob, W. Rossow, G. Tselioudis, and J. Brown (2011), Major characteristics of southern ocean cloud regimes and their effects on the energy budget, *J. Clim.*, **24**(19), 5061–5080.

Haynes, J. M., T. H. Vonder Harr, T. L'Ecuyer, and D. Henderson (2013), Radiative heating characteristics of Earth's cloudy atmosphere from vertically resolved active sensors, *Geophys. Res. Lett.*, **40**, 624–630, doi:10.1002/grl.50145.

Henderson, D. S., T. L'Ecuyer, G. Stephens, P. Partain, and M. Sekiguchi (2013), A multi-sensor perspective on the radiative impacts of clouds and aerosols, *J. Appl. Meteorol. Climatol.*, **52**, 853–871, doi:http://dx.doi.org/10.1175/JAMC-D-12-025.1.

Joiner, J., A. P. Vasilkov, P. K. Bhartia, G. Wind, S. Platnick, and W. P. Menzel (2010), Detection of multilayer and vertically extended clouds using A-Train sensors, *Atmos. Meas. Tech.*, **3**, 233–247.

King, M. D., S. Platnick, W. P. Menzel, S. A. Ackerman, and P. A. Hubanks (2013), Spatial and temporal distribution of clouds observed by MODIS onboard the Terra and Aqua satellites, *IEEE Trans. Geosci. Remote Sens.*, **51**, 3826–3852.

L'Ecuyer, T. S., N. B. Wood, T. Haladay, G. L. Stephens, and P. W. Stackhouse Jr. (2008), Impact of clouds on atmospheric heating based on the R04 CloudSat fluxes and heating rates data set, J. Geophys. Res. Atmos., **113**, D00A15, doi:10.1029/2008JD009951.

L'Ecuyer, T. S., and J. H. Jiang (2010), Touring the atmosphere aboard the A-Train, *Phys. Today*, **63**(7), 36–41, doi:10.1063/1.3463626.

Leinonen, J., M. D. Lebsock, L. Oreopoulos, and N. Cho (2016), Interregional differences in MODIS-derived cloud regimes, *J. Geophys. Res. Atmos.*, **121**, 11,648–11,665, doi:10.1002/2016JD025193.

Li, J., J. Huang, K. Stamnes, T. Wang, Q. Lv, and H. Jin (2015), A global survey of cloud overlap based on CALIPSO and CloudSat measurements, *Atmos. Chem. Phys.*, 15, 519-536, doi:10.5194/acp-15-519-2015.

Mace, G. G., Q. Zhang, M. Vaughan, R. Marchand, G. Stephens, C. Trepte, and D. Winker (2009), A description of hydrometeor layer occurrence statistics derived from the first year of

merged Cloudsat and CALIPSO data, *J. Geophys. Res.*, **114**, D00A26, doi:10.1029/2007JD009755.

Mace, G. G., and F. J. Wrenn (2013), Evaluation of the hydrometeor layers in the East and West Pacific within ISCCP cloud-top pressure-optical depth bins using merged CloudSat and CALIPSO data, *J. Clim.*, **26**, 9429–9444, doi:10.1175/JCLI-D-12-00207.1.

Mace, G. G., and Q. Zhang (2014), The CloudSat radar-lidar geometrical profile product (RL-GeoProf): Updates, improvements, and selected results, *J. Geophys. Res. Atmos.*, **119**, 9441–9462, doi:10.1002/2013JD021374.

Mason, S., C. Jakob, A. Protat, and J. Delanoë (2014), Characterizing observed midtopped cloud regimes associated with southern ocean shortwave radiation biases, *J. Clim.*, **27**(16), 6189–6203, doi:10.1175/jcli-d-14-00139.1.

Matus, A. V. and T. S. L'Ecuyer (2017), The role of cloud phase in Earth's radiation budget, *J. Geophys. Res. Atmos.*, **122**, 2559–2578, doi:10.1002/2016JD025951.

Nazaryan, H., M. P. McCormick, and W. P. Menzel (2008), Global characterization of cirrus clouds using CALIPSO data, J. Geophys. Res., 113, D16211, doi:10.1029/2007JD009481.

Norris, J. R., and C. Leovy (1994), Interannual variability in stratiform cloudiness and sea surface temperature, *J. Clim.*, **7**, 1915–1925.

Oreopoulos, L., and R. Davies (1993), Statistical dependence of albedo and cloud cover on sea surface temperature for two tropical marine stratocumulus regions, *J. Clim.*, **6**, 2434–2447.

Oreopoulos, L., and W. B. Rossow (2011), The cloud radiative effects of International Satellite Cloud Climatology Project weather states, *J. Geophys. Res.*, **116**(D12), D12202, doi:10.1029/2010JD015472.

Oreopoulos, L., D. Lee, Y. C. Sud, and M. J. Suarez (2012), Radiative impacts of cloud heterogeneity and overlap in an atmospheric general circulation model, *Atmos. Chem. Phys.*, **12**, 9097–9111.

Oreopoulos, L., N. Cho, D. Lee, S. Kato, and G. J. Huffman (2014), An examination of the nature of global MODIS cloud regimes, *J. Geophys. Res. Atmos.*, **119**, 8362–8383, doi:10.1002/2013JD021409.

Oreopoulos, L., N. Cho, D. Lee, and S. Kato (2016), Radiative effects of global MODIS cloud regimes, *J. Geophys. Res. Atmos.*, **121**, 2299–2317, doi:10.1002/2015JD024502.

Oreopoulos, L., N. Cho, and D. Lee (2017), Using MODIS Cloud Regimes to Sort Diagnostic Signals of Aerosol-Cloud-Precipitation Interactions, *J. Geophys. Res. Atmos*., **122**, doi:10.1002/2016JD026120.

Platnick, S., et al. (2016), The MODIS cloud optical and microphysical products: Collection 6 updates and examples from Terra and Aqua, *IEEE Trans. Geosci. Remote Sens.*, **55**, 502–525, doi:10.1109/TGRS.2016.2610522.

Rossow, W. B., and L. C. Garder (1993), Cloud detection using satellite measurements of infrared and visible radiances for ISCCP, *J. Clim.*, **6**, 2341–2369, doi:10.1175/1520-0442.

Rossow, W., G. Tselioudis, A. Polak, and C. Jakob (2005), Tropical climate described as a distribution of weather states indicated by distinct mesoscale cloud property mixtures, *Geophys. Res. Lett.*, **32**, L21812, doi:10.1029/2005GL024584.

Sassen, K., and Z. Wang (2012), The clouds of the middle troposphere: Composition, radiative impact, and global distribution, *Surv. Geophys.*, **33**(3–4), 677–691, doi:10.1007/s10712-011-9163-x.

Shonk, J., R. Hogan, G. Mace, and J. Edwards (2010), Effect of improving representation of horizontal and vertical cloud structure on the Earth's global radiation budget. Part I: Review and parametrization, *Q. J. R. Meteorol. Soc.*, **136**, 1191–1204.

Stephens, G., et al. (2002), The CloudSat mission and the A-train, *Bull. Am. Meteorol. Soc.*, **83**, 1771–1790.

Tselioudis, G., W. Rossow, Y.-C. Zhang, and D. Konsta (2013), Global weather states and their properties from passive and active satellite cloud retrievals, *J. Clim.*, **26**, 7734–7746, doi:10.1175/JCLI-D-13-00024.1.

Wang, T., E. J. Fetzer, S. Wong, B. H. Kahn, and Q. Yue (2016), Validation of MODIS cloud mask and multilayer flag using CloudSat-CALIPSO cloud profiles and a cross-reference of their cloud classifications, J. Geophys. Res. Atmos., **121**, 11,620–11,635, doi:10.1002/2016JD025239.

Wind, G., S. Platnick, M. D. King, P. A. Hubanks, B. A. Baum, M. J. Pavolonis, A. K. Heidinger, P. Yang, and D. P. Kratz (2010), Multilayer cloud detection with MODIS near-infrared water vapour absorption band, *J. Appl. Meteorol. Climatol.*, **49**, 2315–2333, doi:10.1175/2010JAMC2364.1.

Winker, D. M., et al. (2010), The CALIPSO Mission. A Global 3D view of aerosols and clouds, *Bull. Amer. Meteorol. Soc.*, **91**(9), 1211–1229, doi:10.1175/2010bams3009.1.

Yuan, T., and L. Oreopoulos (2013), On the global character of overlap between low and high clouds, *Geophys. Res. Lett.*, **40**, 5320–5326, doi:10.1002/grl.50871.

Zhang, D., Z. Wang, and D. Liu (2010), A global view of midlevel liquid-layer topped stratiform cloud distribution and phase partition from CALIPSO and CloudSat measurements, *J. Geophys. Res.*, **115**, D00H13, doi:10.1029/2009JD012143.

Figure 1.

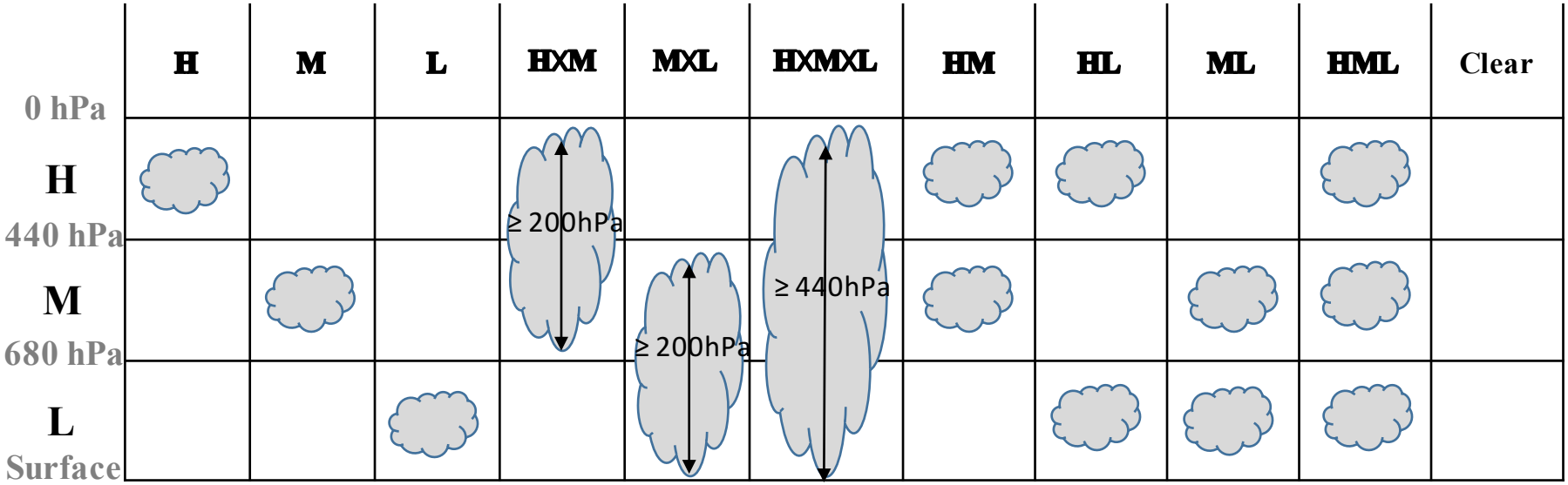
H
M
L
HXM
MXL
HXMXL
HM
HL
ML
HML
Clear
0 hPa
H
440 hPa
M
680 hPa
L
Surface
≥ 200hPa
≥ 200hPa
≥ 440hPa

Figure 1

Figure 2.

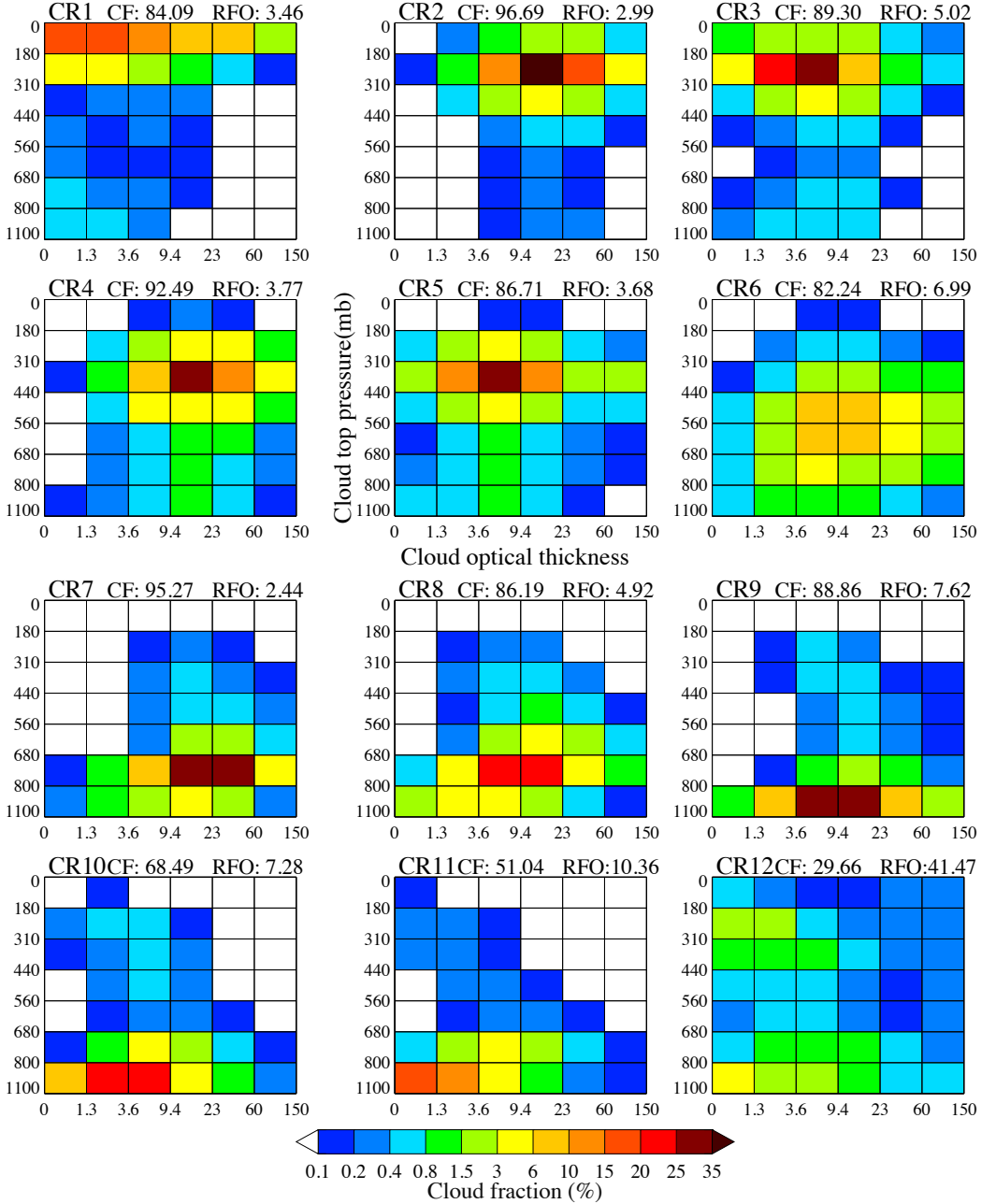
CR1 CF: 84.09 RFO: 3.46
CR2 CF: 96.69 RFO: 2.99
CR3 CF: 89.30 RFO: 5.02
CR4 CF: 92.49 RFO: 3.77
CR5 CF: 86.71 RFO: 3.68
CR6 CF: 82.24 RFO: 6.99
CR7 CF: 95.27 RFO: 2.44
CR8 CF: 86.19 RFO: 4.92
CR9 CF: 88.86 RFO: 7.62
CR10 CF: 68.49 RFO: 7.28
CR11 CF: 51.04 RFO:10.36
CR12 CF: 29.66 RFO:41.47
Cloud top pressure(mb)
0 180 310 440 560 680 800 1100
Cloud optical thickness
0 1.3 3.6 9.4 23 60 150
0.1 0.2 0.4 0.8 1.5 3 6 10 15 20 25 35
Cloud fraction (%)

Figure 3.

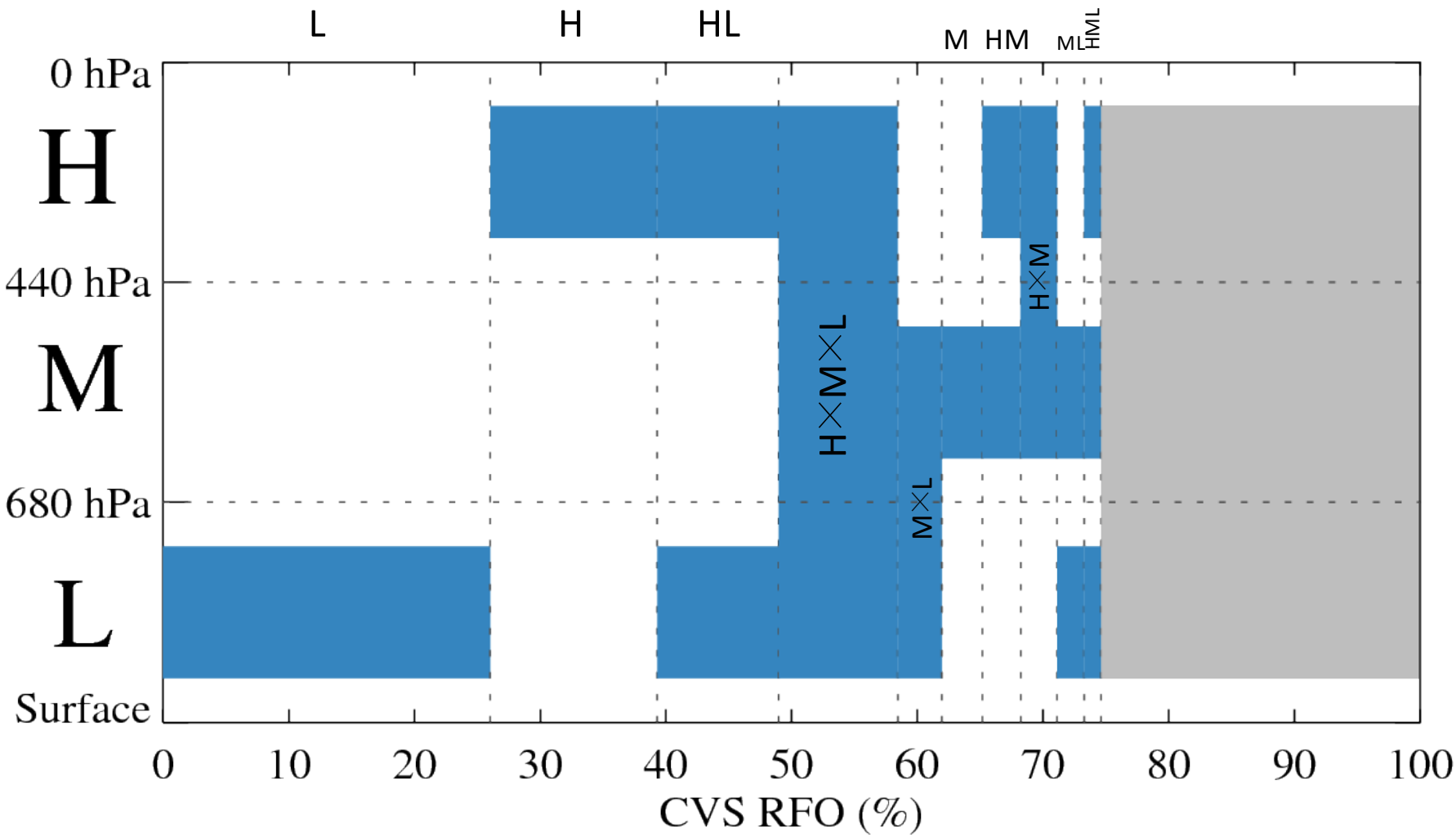
L
H
HL
M
HM
ML
HML
0 hPa
H
440 hPa
M
680 hPa
L
Surface
H×M×L
H×M
M×L
0
10
20
30
40
50
60
70
80
90
100
CVS RFO (%)

Figure 3

Figure 4.

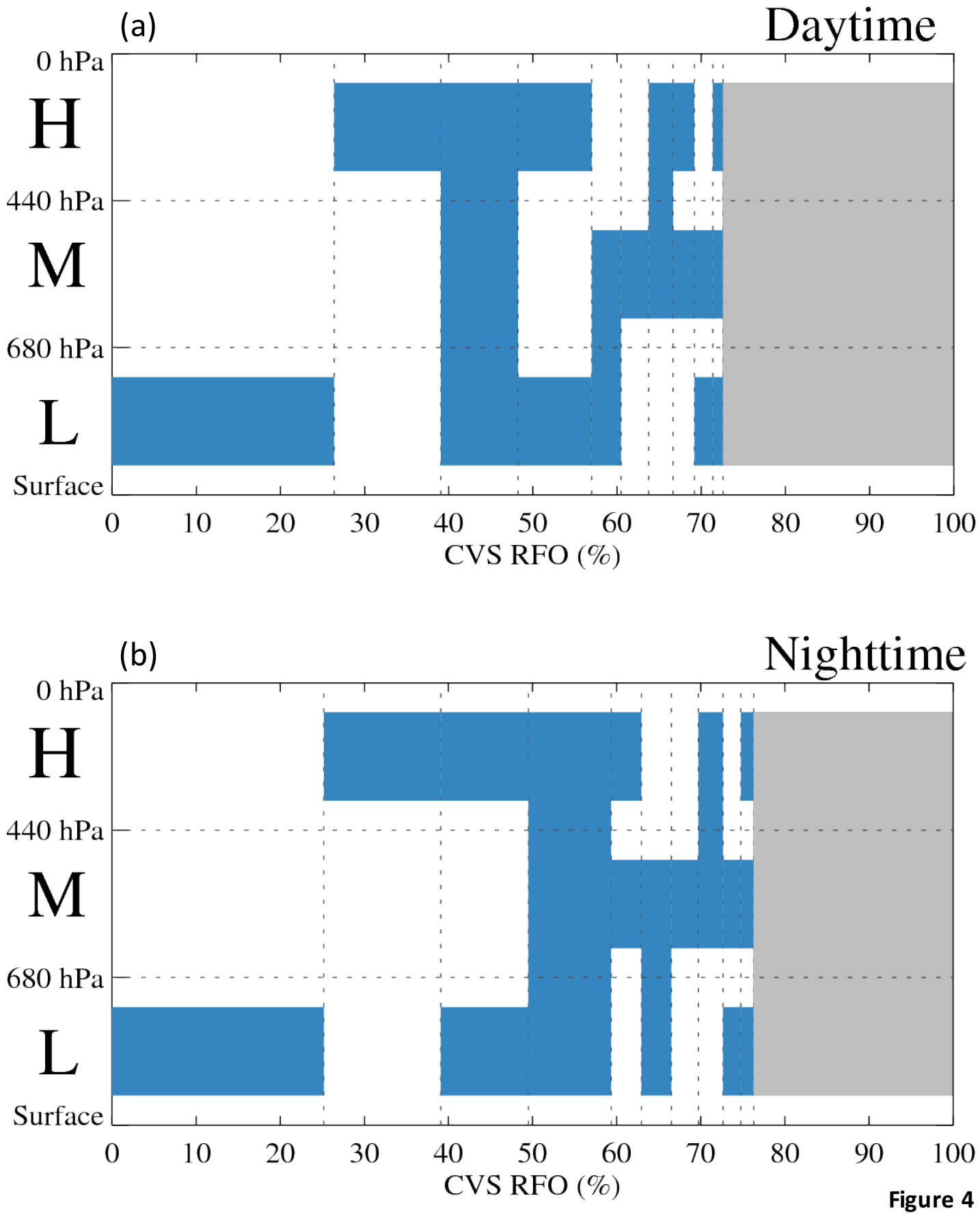
(a)
Daytime
0 hPa
H
440 hPa
M
680 hPa
L
Surface
0
10
20
30
40
50
60
70
80
90
100
CVS RFO (%)
(b)
Nighttime
0 hPa
H
440 hPa
M
680 hPa
L
Surface
0
10
20
30
40
50
60
70
80
90
100
CVS RFO (%)

Figure 4

Figure 5.

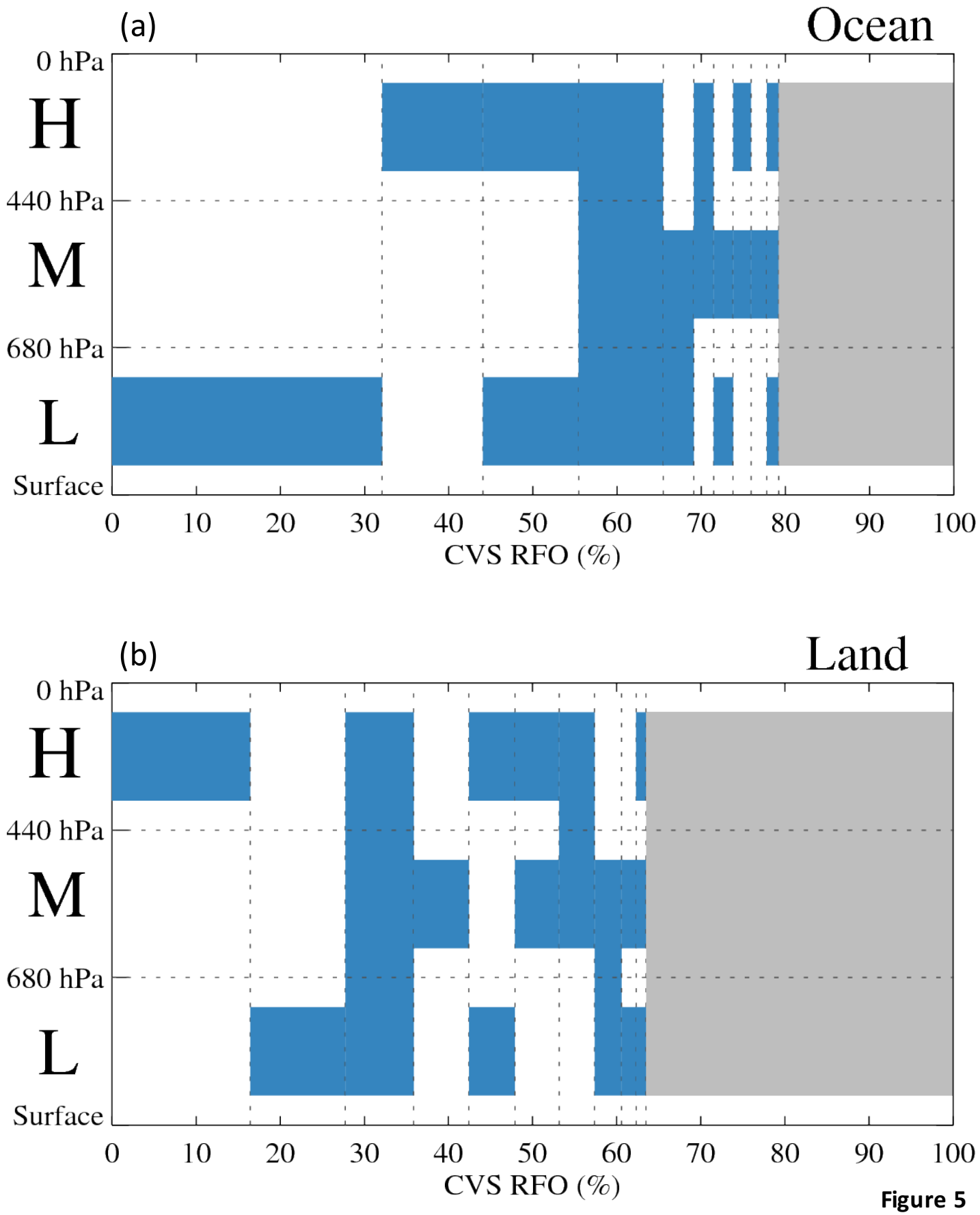
(a)
Ocean
0 hPa
H
440 hPa
M
680 hPa
L
Surface
0
10
20
30
40
50
60
70
80
90
100
CVS RFO (%)
(b)
Land
0 hPa
H
440 hPa
M
680 hPa
L
Surface
0
10
20
30
40
50
60
70
80
90
100
CVS RFO (%)

Figure 5

Figure 6.

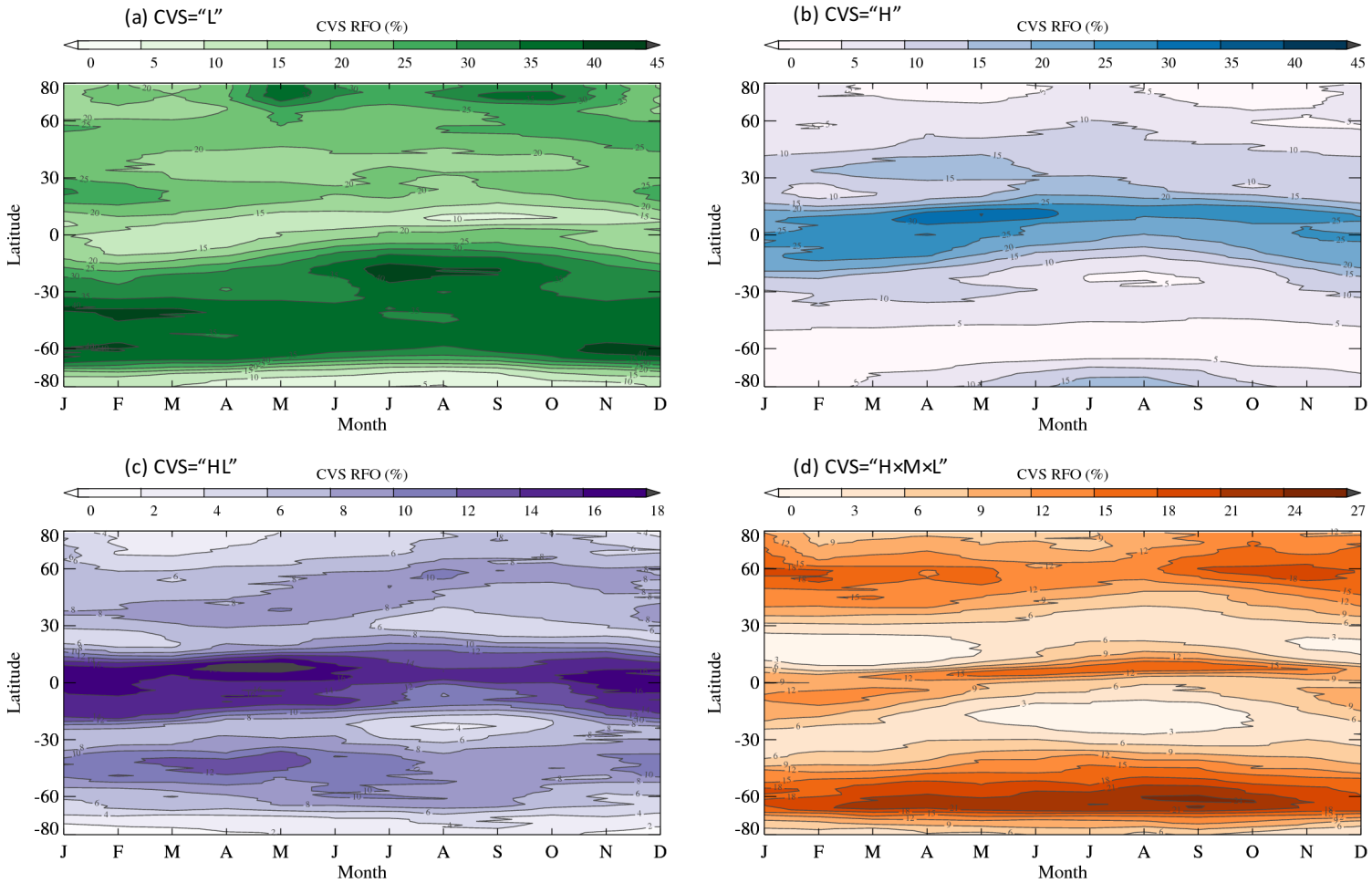
(a) CVS="L"
CVS RFO (%)
0 5 10 15 20 25 30 35 40 45
(b) CVS="H"
CVS RFO (%)
0 5 10 15 20 25 30 35 40 45
(c) CVS="HL"
CVS RFO (%)
0 2 4 6 8 10 12 14 16 18
(d) CVS="H×M×L"
CVS RFO (%)
0 3 6 9 12 15 18 21 24 27
Latitude
80 60 30 0 -30 -60 -80
Month
J F M A M J J A S O N D

Figure 6

Figure 7.

Figure 7

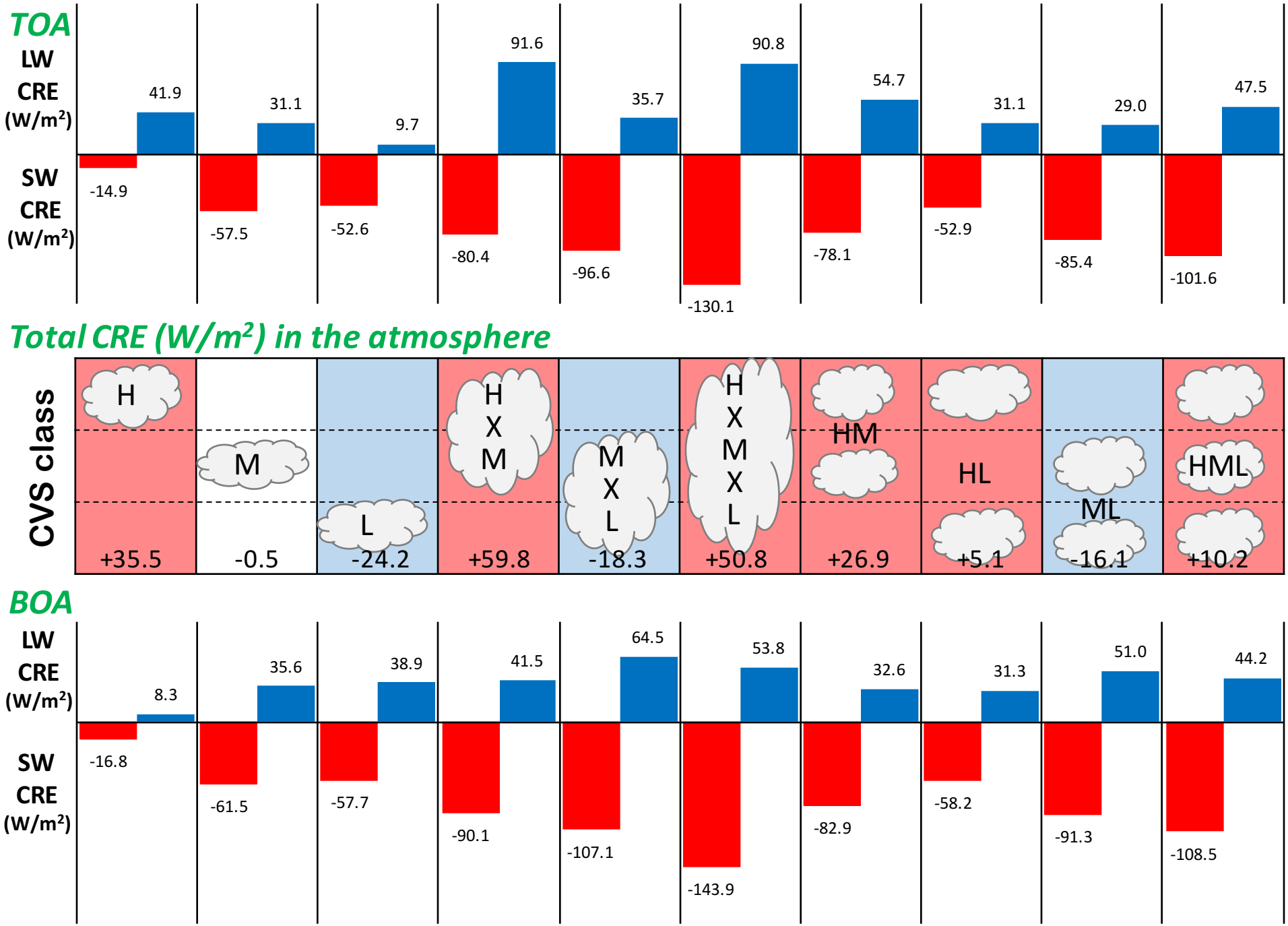
TOA
LW CRE (W/m²)
SW CRE (W/m²)
41.9
31.1
9.7
91.6
35.7
90.8
54.7
31.1
29.0
47.5
-14.9
-57.5
-52.6
-80.4
-96.6
-130.1
-78.1
-52.9
-85.4
-101.6
Total CRE (W/m²) in the atmosphere
CVS class
H
M
L
H X M
M X L
H X M X L
HM
HL
ML
HML
+35.5
-0.5
-24.2
+59.8
-18.3
+50.8
+26.9
+5.1
-16.1
+10.2
BOA
LW CRE (W/m²)
SW CRE (W/m²)
8.3
35.6
38.9
41.5
64.5
53.8
32.6
31.3
51.0
44.2
-16.8
-61.5
-57.7
-90.1
-107.1
-143.9
-82.9
-58.2
-91.3
-108.5

Figure 8.

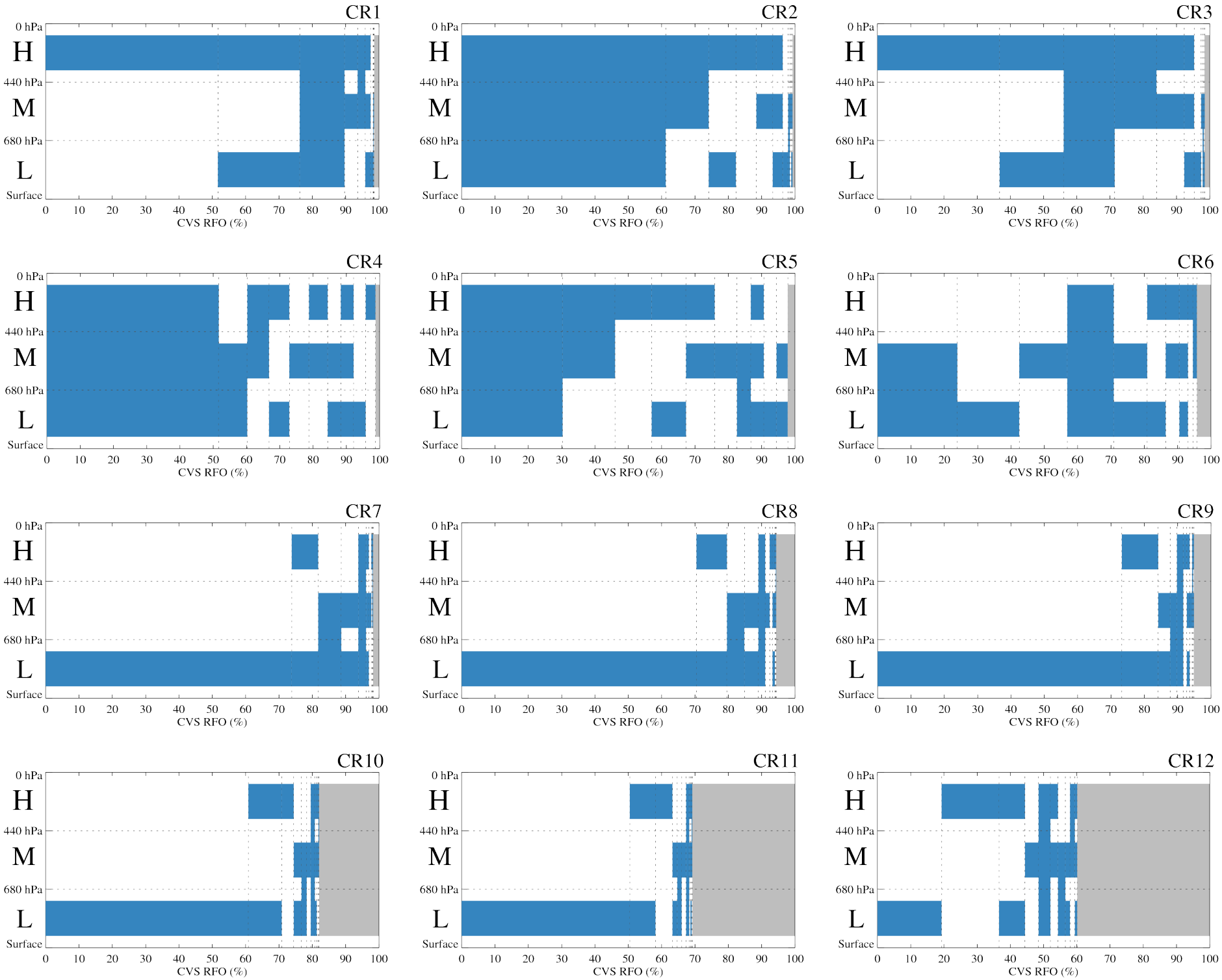
CR1
CR2
CR3
CR4
CR5
CR6
CR7
CR8
CR9
CR10
CR11
CR12
0 hPa
440 hPa
680 hPa
Surface
H
M
L
0 10 20 30 40 50 60 70 80 90 100
CVS RFO (%)

Figure 8

Figure 9.

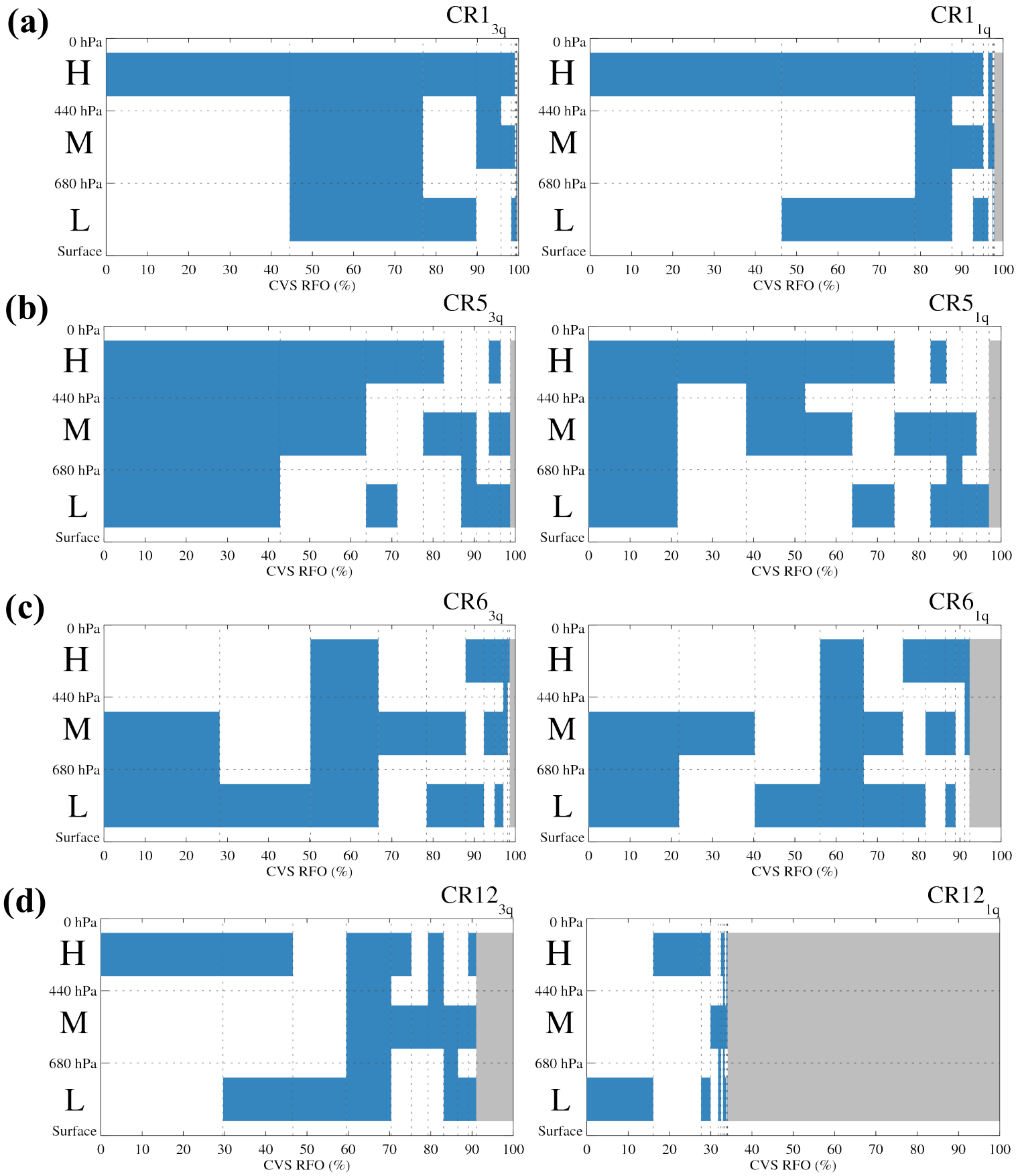
(a)
CR1 3q
CR1 1q
(b)
CR5 3q
CR5 1q
(c)
CR6 3q
CR6 1q
(d)
CR12 3q
CR12 1q
0 hPa
440 hPa
680 hPa
Surface
H
M
L
0 10 20 30 40 50 60 70 80 90 100
CVS RFO (%)

Figure 9

Appendix Figure 1.

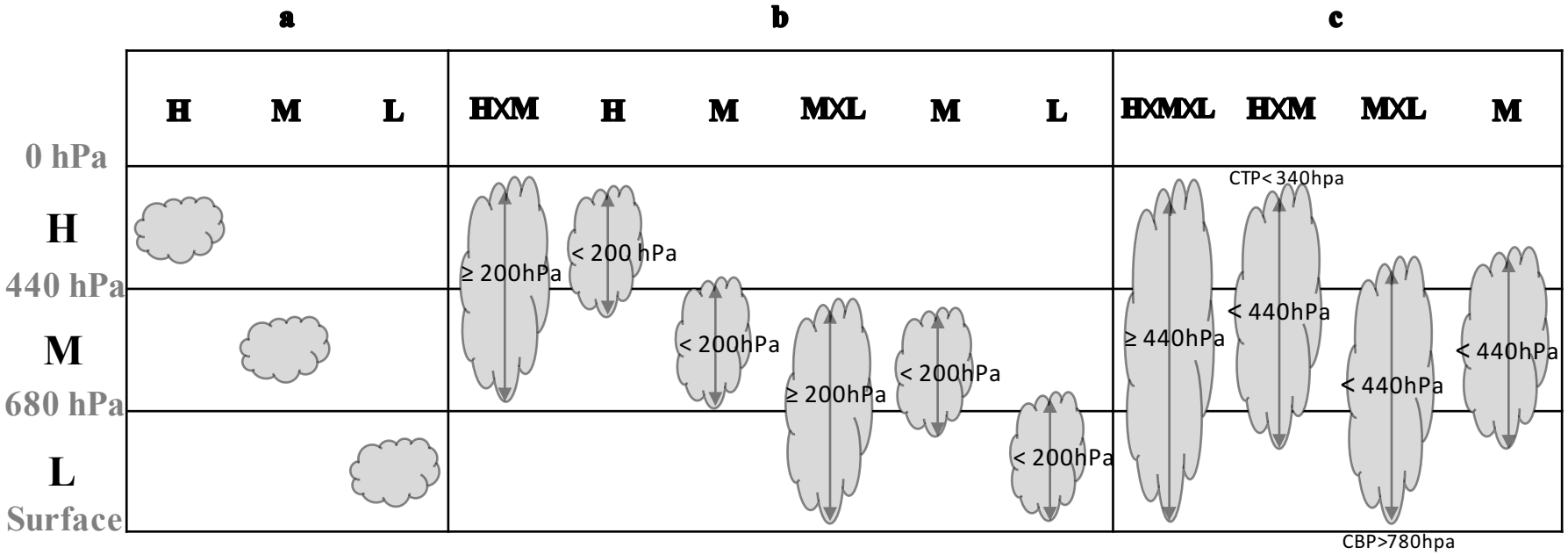
a
b
c
H
M
L
HXM
H
M
MXL
M
L
HXMXL
HXM
MXL
M
0 hPa
H
440 hPa
M
680 hPa
L
Surface
≥ 200hPa
< 200 hPa
< 200hPa
≥ 200hPa
< 200hPa
< 200hPa
≥ 440hPa
CTP< 340hpa
< 440hPa
< 440hPa
< 440hPa
CBP>780hpa

Figure A1

Appendix Figure 2.

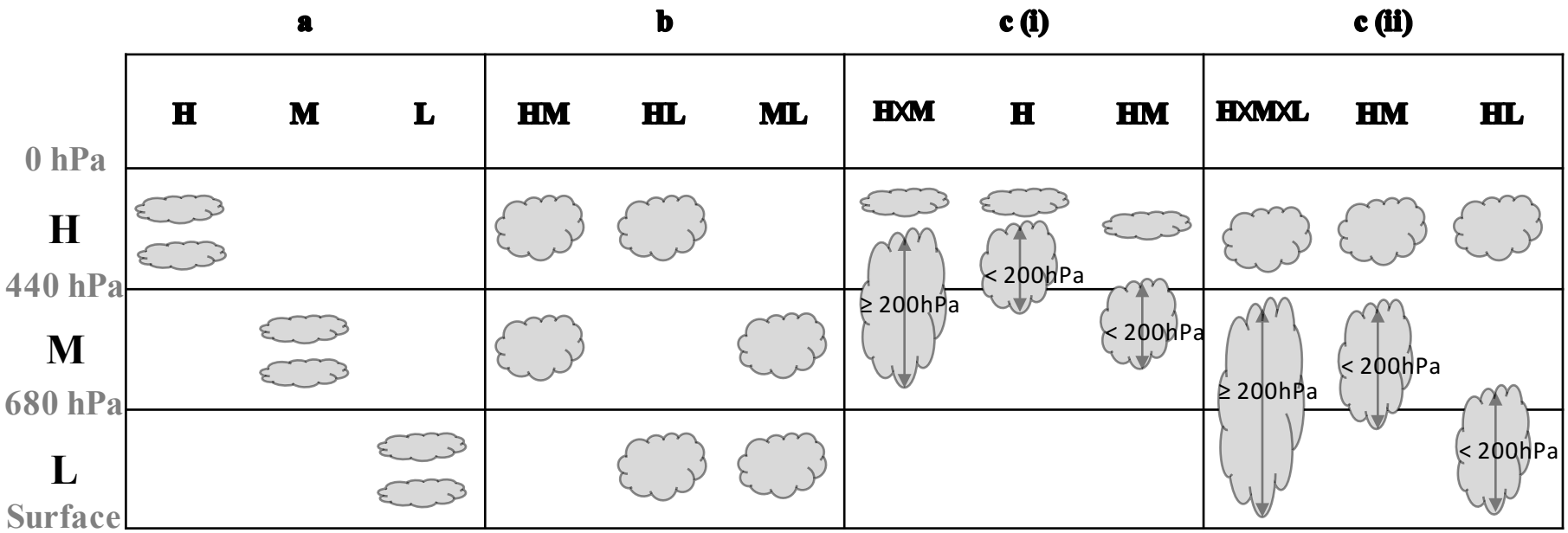
a
b
c (i)
c (ii)
H
M
L
HM
HL
ML
HXM
H
HM
HXMXL
HM
HL
0 hPa
H
440 hPa
M
680 hPa
L
Surface
≥ 200hPa
< 200hPa
< 200hPa
≥ 200hPa
< 200hPa
< 200hPa

Figure A2

Appendix Figure 3.

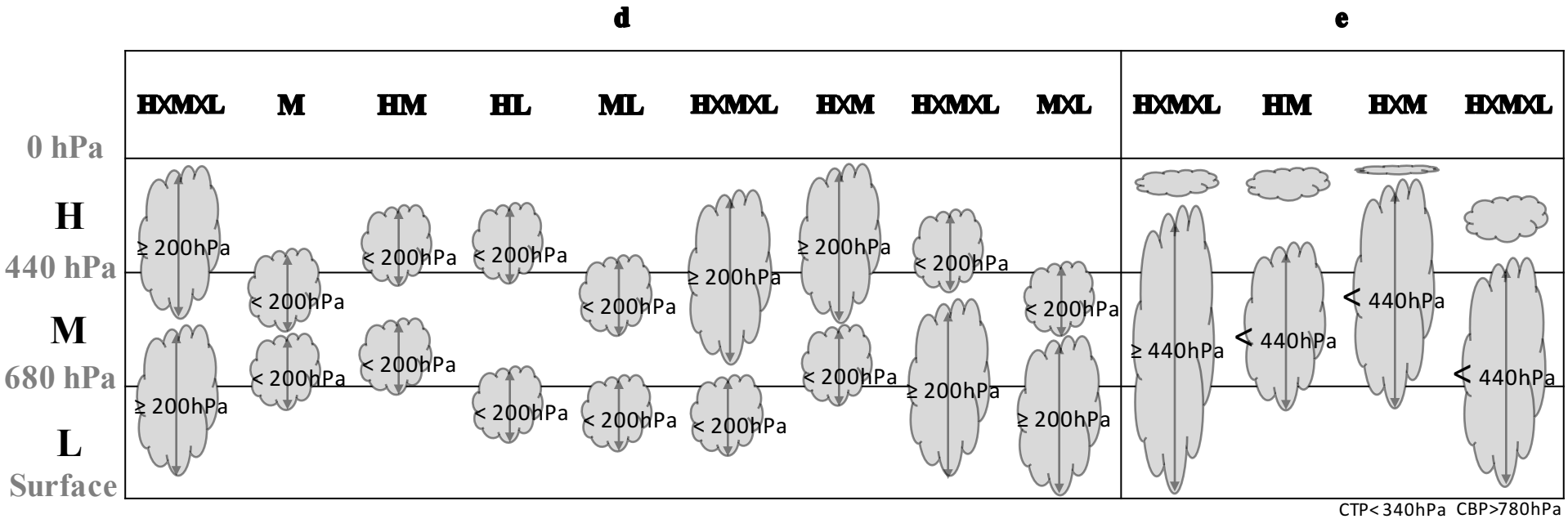
d
e
HXMXL
M
HM
HL
ML
HXMXL
HXM
HXMXL
MXL
HXMXL
HM
HXM
HXMXL
0 hPa
H
440 hPa
M
680 hPa
L
Surface
≥ 200hPa
< 200hPa
≥ 440hPa
< 440hPa
CTP< 340hPa CBP>780hPa

Figure A3

Appendix Figure 4.

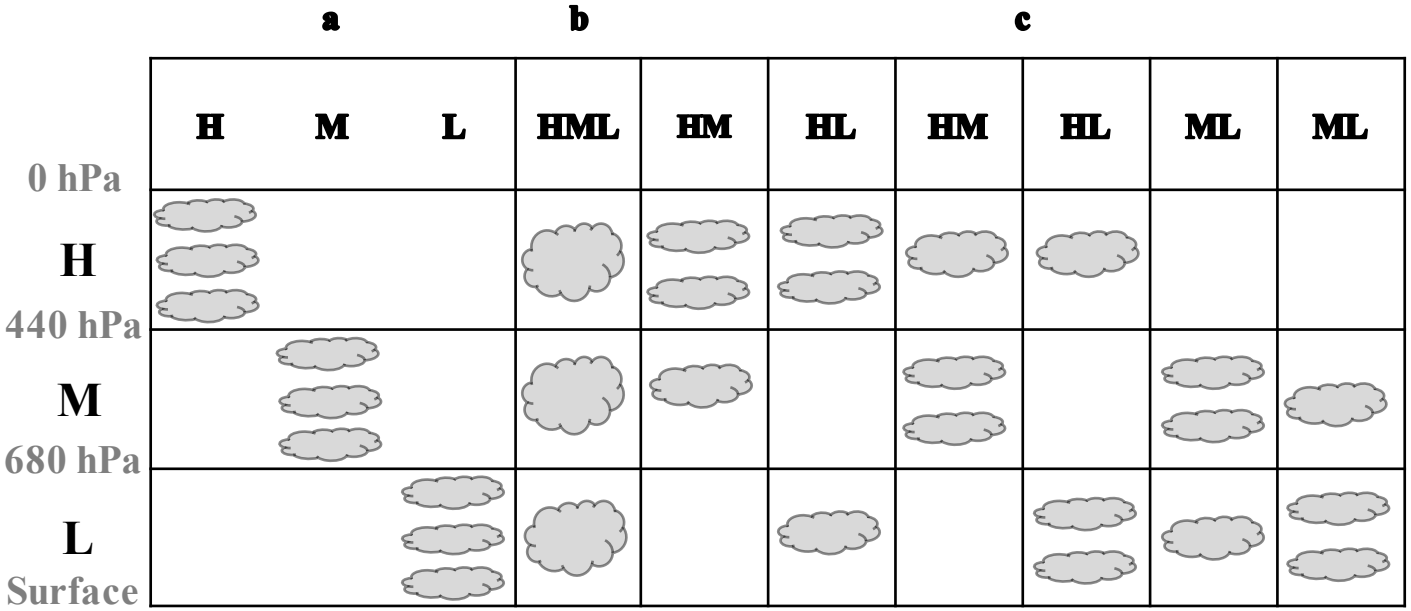

Figure A4